UPPSALA
UNIVERSITET

ELEKTRO-MFE 20005
Examensarbete 30 hp
Juni 2020

Design and Development of a Measurement System to Track the Motion of a Point Absorber

Juliana Lüer

Masterprogram i förnybar elgenerering
Master Programme in Renewable Electricity Production

UPPSALA
UNIVERSITET

Teknisk- naturvetenskaplig fakultet
UTH-enheten

Besöksadress:
Ångströmlaboratoriet
Lägerhyddsvägen 1
Hus 4, Plan 0

Postadress:
Box 536
751 21 Uppsala

Telefon:
018 – 471 30 03

Telefax:
018 – 471 30 00

Hemsida:
http://www.teknat.uu.se/student

Abstract

Design and Development of a Measurement System to Track the Motion of a Point Absorber

Juliana Lüer

Because of climate change renewable energy field is becoming more and more relevant. Renewable energy can be gained from the sun, from wind but also from ocean waves. To support the research and development in this field reliably measured wave data is collected through a measurement system that shows the exact position of a buoy.

The project consists of the design, development and implementation of such a measurement system. It is divided into three subtasks:
- The power supply based on a solar panel and a battery
- The measurement part including a sensor and its implementation to the circuit
- The deployment of a module for data transmission and communication between the measurement system and the on-shore computer

The power supply is capable to power the system and to maintain the battery voltage. A suggested stronger power supply will be used in a later state of the project to increase the reliability. The results of the charging test are good. The power supply system is connected to the circuit and the battery charges.

For the measurement system the altitude and heading reference system (AHRS) "Ellipse2-D" from SBG Systems has been selected and connected to an Arduino Mega 2560. The AHRS provides raw data and values processed by a Kalman filter. Both data sets are picked up by the microcontroller. The raw data is backed up on a secure digital memory card (SD-card). For the evaluation of the sensor unit, static and dynamic tests are applied to the sensor. In the end it can be seen that the measurement series are aligned with each other.

The information from the Kalman model of the AHRS is transmitted with the Adeunis ARF868 ultra-long range (ULR) modem. The transmitter is linked to the Arduino Mega 2560 and the sensor data is transmitted to the receiver. The first field test already shows the reliability of the system for a range of about 3 km.

The results of the tests are as expected and in the future this system will be implemented on a buoy.

Keywords: accelerometer, AHRS, battery, buoy, data transmission, GNSS, gyroscope, IMU, solar panel, wave energy

Handledare: Irina Temiz
Ämnesgranskare: Jens Engström
Examinator: Mikael Bergkvist
ELEKTRO-MFE 20005

Acknowledgements

I would first like to thank my supervisor Irina Temiz from Uppsala University for her guidance during my studies as my program director and the support and input during my thesis: Thank you for the offline and online meetings, the communication with the university due to the Corona-lab-struggle and the space in your office for my “small” system box during the battery tests. I also want to thank you for the day we spent together testing my system by driving 30 times up and down with the elevator, dropping me off in the nature and driving around to test my data communication and loaning your bike to me to cycle around the lake while you were watching my system. Thank you also for your input during the writing process.

I would also like to acknowledge Jens Engström of Uppsala University as the subject reader of my thesis. Thank you for your very valuable comments on this thesis.

I would also like to thank the team from SBG Systems for their support. Thank you, Sébastien Manigot for the fast help and shipment. Especially, I want to thank Vincent Peyrin who answered me every question I had and explained so many things to me during the training sessions. Merci beaucoup!

Also, I would like to thank Juan de Santiago for the support during the organisation of the presentation and the helpful guidance during my studies as my study counsellor and Linn Eriksson who opened me the doors in the university buildings.

Anna, ich möchte mich auch bei Dir bedanken. Vielen lieben Dank dafür, dass ich Dich als Englisch-Korrekturleserin hatte!

Zu guter Letzt möchte ich Euch danken, Mama, Papa und Dominic für Eure Unterstützung während meiner Studienzeit, aber vor allem jetzt, während meiner Masterarbeit. Danke, dass ihr so viele Stunden und Abende geopfert habt zum Korrekturlesen!

Table of Content

List of Figures

List of Tables

Abbreviations

AC	*Alternating Current*
Acc	*Accelerometer*
ADC	*Analogue-Digital-Converter*
AHRS	*Attitude and Heading Reference System*
AM	*Amplitude Modulation*
BDS	*BeiDou Navigation Satellite System*
CLK	*Clock*
CMOS	*Complementary metal–oxide–semiconductor*
COM port	*Communication port*
CR	*Carriage Return*
CS	*Chip Select*
DC	*Direct Current*
DI	*Data In*
DO	*Data Out*
DOF	*Degrees of Freedom*
ECI	*Earth-Centred Inertial*
EMEC	*European Marine Energy Centre*
FM	*Frequency Modulation*
GLONASS	*Global'naya Navigatsionnaya Sputnikovaya Sistema (Global Navigation Satellite System)*
GNSS	*Global Navigation Satellite System*
GPS	*Global Positioning System*
Gyro	*Gyroscope*
HF	*High Frequency*
IC	*Integrated Circuit*
IMU	*Inertial Measurement Unit*
INS	*Inertial Navigation System*

LED	*Light-Emitting Diode*
LF	*Line Feed*
LIDAR	*Light Detection and Ranging*
MEMS	*Micro Electro Mechanical Systems*
MISO	*Master In Slave Out*
MOSI	*Master Out Slave In*
MPPT	*Maximum Power Point Tracking*
NAVSTAR GPS	*Navigational Satellite Timing and Ranging – Global Positioning System*
NMEA	*National Marine Electronics Association*
OS	*Operating System*
OWC	*Oscillating Water Column*
PCB	*Printed Circuit Board*
PV	*Photovoltaic*
PWM	*Pulse Width Modulation*
RF	*Radio Frequency*
ROV	*Remotely Operated underwater Vehicle*
RTK	*Real Time Kinematic*
SCK	*Serial Clock*
SD-card	*Secure Digital Memory Card*
SOC	*State of Charge*
SPI	*Serial Peripheral Interface*
SS	*Slave Select*
TRL	*Technology Readiness Levels*
TTL	*Transistor-Transistor-Logic*
UHF	*Ultra-High Frequency*
ULR	*Ultra-Long Range*
USB	*Universal Serial Bus*

UTC	*Coordinated Universal Time*
WEC	*Wave Energy Converter*
Wi-Fi	*Wireless Fidelity*
9D	*Nine-Dimensional*

1 Introduction

1.1 Background

“Global warming”, “fossil fuel” and “reduction of the greenhouse gas emissions” are all keywords and headlines from the news in the last years. With this in mind, it is inevitable that renewable electricity production gets more and more important in the future.

Wind power, hydropower and also solar power are meanwhile far developed and already established technologies. But there are still more possibilities on Earth to gain energy.

One important and available resource is the ocean – wave energy. Waves are caused by the wind that arouses the water surface by blowing over it. Offshore 120-190 TWh/year are estimated for the energy potential that is available only in the European Union region. (1) The development to extract electric power from wave energy is still a very active field.

1.2 Ocean Measurement Technologies

The ocean climate is rough and it is difficult to install and to maintain applications in the ocean. Also, there are different parameters influencing the energy extraction: wave height, wavelength, wave speed and water density, as well as the wave conversion technology itself. (1) Due to this, it is necessary to do more research on this energy source; especially with focus on ocean measurement technologies.

There are different systems available on the market; to name a few: subsurface or platform based instrumentations, buoys and high frequency (HF) radar measurements. (1)

Subsurface instrumentations include systems like pressure sensors. If water gets deeper, the pressure increases. A pressure sensor fixed to the seabed or a pile uses this phenomenon to measure the wave height. To improve the results another pressure sensor that measures the air pressure is needed. Issues may arise since the wave frequency has an influence on the underwater pressure. This system is unreliable for short waves. Another technology that is used in this category is an echo sounder. This is placed under water and faces the water surface. It sends out sound waves that are reflected from the water surface and measures the time until the reflection travelled back (see equivalent system chapter 2.2.1). However, in stormy waves the echo sounder can produce erroneous results due to reflection of the ultrasonic waves from air bubbles contained in the water. More information can be seen in (1, 2).

Platform based instrumentations are systems that have to be fixed to a pile or a platform. For instance, wave staffs belong to this category. The system consists of a vertical gauge that is half-submerged and is fixed to a pile. It measures the wave height. Along the whole gauge it has open electrodes. Due to an up and down movement of the water surface, more or less electrodes get short-circuited by the water. This changes the resistance which can be measured. (1)

A **wave measurement buoy** has the advantage that it does not need a fixed structure like a platform or a pile and is not submerged deep in the water. Cheaper systems just measure the heave motion (see chapter 2.1) with the help of an accelerometer (see chapter 2.3.1). More advanced systems can track the motion in all six degrees of freedom (DOF) (see chapter 2.1) with the help of accelerometers and gyroscopes (see chapter 2.3.2), commonly called inertial measurement unit (IMU) (see chapter 2.2.3). Mostly, these sensors are combined with a global

positioning system (GPS) (see chapter 2.3.4) to increase the accuracy of the measurement. This also helps to avoid that the clock drifts and to be able to process the data further. These systems are often merged in attitude and heading reference systems (AHRS) or inertial navigation systems (INS) (see chapter 2.2.4).

High frequency (HF) radar are used to measure mainly the ocean current in a larger area close to the shore. (1, 3) At the coast, HF antennas are installed. (1) These send HF-waves which are backscattered by the waves. Depending on the different characteristics of the wave, different parameter of the HF-signal have been changed and can be analysed. (1, 3)

1.3 Wave Energy Converters

To extract the wave energy and produce electric power, there is already a large number of wave energy converters (WEC) at different technology readiness levels (TRL) available that can be characterised in different categories. (1)

Regarding to the European marine energy centre (EMEC) there are following classifications: oscillating water columns, overtopping systems, attenuators, point absorbers, submerged pressure differential, oscillating wave surge converter, bulge wave and rotating mass. (4)

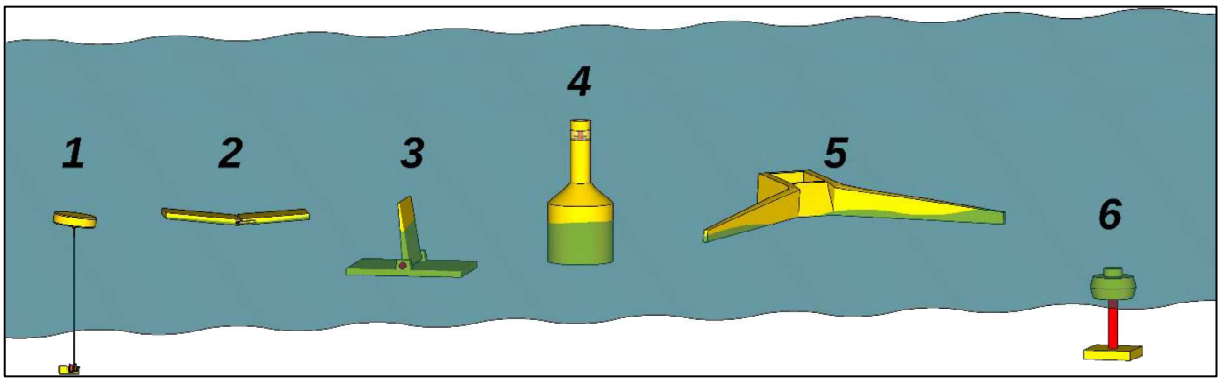

Figure 1: Different WEC concepts (1: point absorber; 2: attenuator; 3: oscillating wave surge converter; 4: oscillating water column: 5: overtopping device; 6: submerged pressure differential)[1].

Oscillating water columns (OWC) are wave energy devices that can be used floating or fixed to the shore. Examples are LIMPET which was tested in Islay, Scotland (fixed to the shore) or The Mighty Whale which is a floating device tested in the Tokyo Bay. A chamber filled with air and an air turbine in the end is installed. The force of the wave pushes water into the chamber and with this the air above the water surface through the turbine which generates electricity. The oscillating water can actuate it in both movement directions. (see Figure 2) (1, 5)

[1] © Ingvald Straume, Wikimedia, licensed under the Creative Commons CC0 1.0 Universal Public Domain Dedication license, https://commons.wikimedia.org/wiki/File:Wave_energy_concepts_overview_numbered.png, cited 23.06.2020

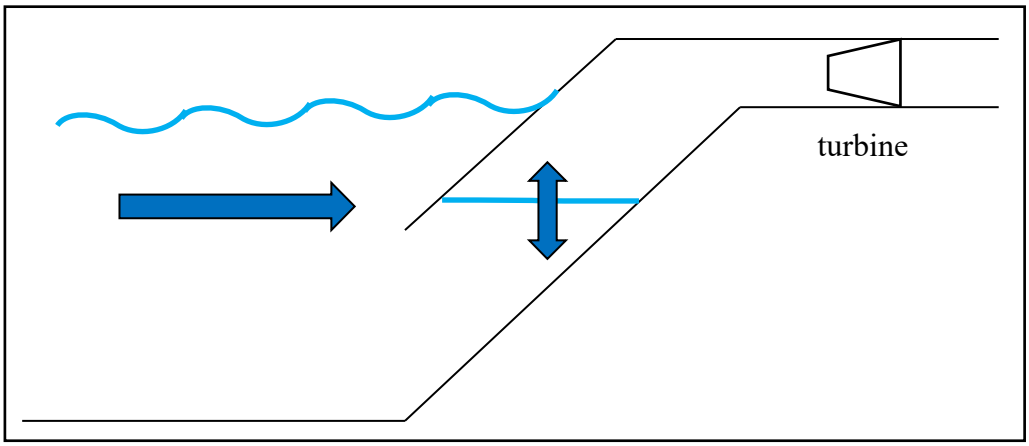

Figure 2: Concept oscillating water column.

Overtopping systems are WEC that are flooded by water. The water reservoir is situated higher than the water surface. Waves are flooding into this and the water excess flows through a turbine back into the ocean. With this, the potential energy of the water is used to extract energy. (see Figure 3) For instance to name, the Norwegian TAPCHAN or the Wave Dragon from Denmark. (1, 6)

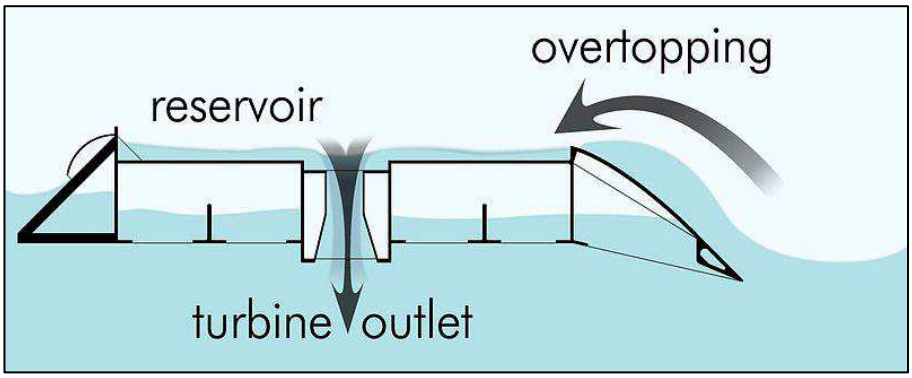

Figure 3: Concept overtopping system[2].

Attenuators (see No. 2 in Figure 1) consist normally of several elements and float on the water surface, for example The Pelamis (see Figure 4) which was tested in Scotland. Due to the motion through the waves the different joints are moved and produce electricity by the usage of hydraulic pumps. The main axis of these devices is parallel to the direction of the waves. (1, 4, 7)

[2] © Erik Friis-Madsen, en.wikipedia, licensed under the Creative Commons Attribution 3.0 Unported license, https://en.m.wikipedia.org/wiki/File:WD_side_princip.JPG, cited 19.06.2020, taken without changes

Figure 4: Pelamis WEC[3].

Point absorbers consist of a floating, moving part (either under water or on the water surface) and a stable underwater construction. The floater can absorb energy from all directions of the wave. Due to the pressure on the floating part (for example on The Archimedes Wave Swing, tested in Portugal, see Figure 5) or the lifting of the floater on top of the wave (for example the American AquaBuOY, see No. 1 in Figure 1), the energy is extracted. This works either through a piston that pushes water through a turbine in the fixed structure or a linear generator that is situated in the stable construction. (1, 4, 8) If the device is submerged and works with the pressure principle, the concept is also called **submerged pressure differential** (see No. 6 in Figure 1 and Figure 5). (8)

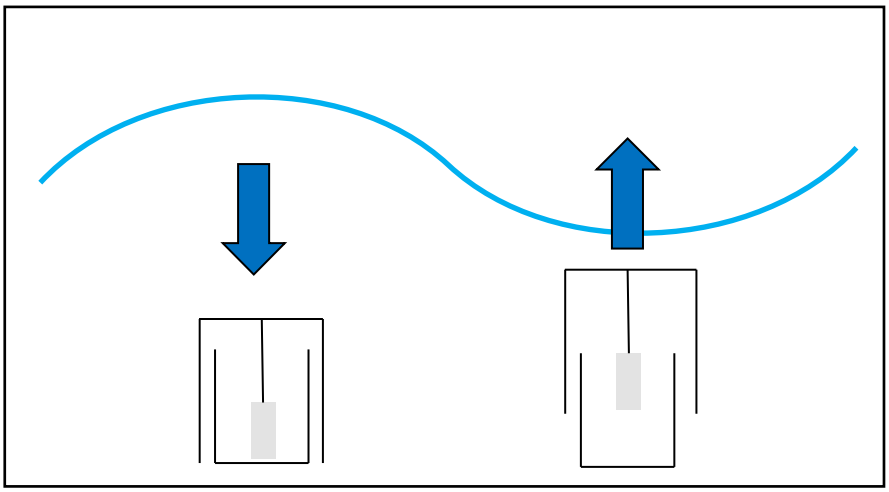

Figure 5: Concept Archimedes wave swing.

Oscillating wave surge converters gain energy from the horizontal surge motion of fluid particles and are installed perpendicular to the direction of the waves. A converter consists of a paddle that is fixed to the seabed as a near shore application and swings with the motion. (see No. 3 in Figure 1) (4, 9, 10) One company that used that concept was Aquamarine Power Ltd. in their Oyster concept. (11)

[3] © P123, Wikimedia, licensed under public domain license, https://commons.wikimedia.org/wiki/File:Pelamis_at_EMEC.jpg. cited 23.06.2020

Bulge wave is a WEC that consist of a long tube that swims directly below the water surface and which is moored on one side. When a wave passes along the pipe, a bulge is created due to pressure variations and pushed to the end of the tube. There, it actuates a turbine. (see Figure 6) Checkmate Seaenergy Limited uses this concept for their Anaconda. (4, 12)

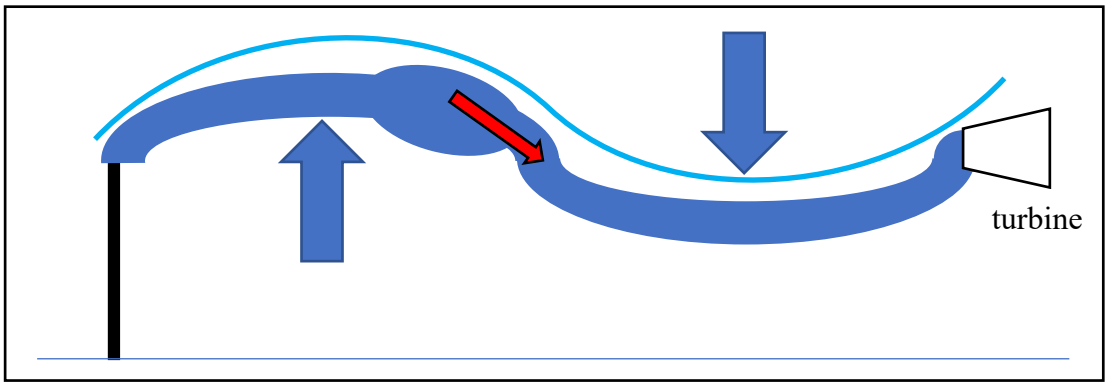

Figure 6: Concept bulge wave.

A **rotating mass** consists of a floating body which contains a weight inside that rotates around an axis. With the heave and sway motion of a wave, the mass starts to rotate inside the floater. (see Figure 7) Due to the rotational motion, an internal generator can produce energy. (4) The Finnish company Wello built a system that is named Penguin that is based on the rotating mass concept. (13)

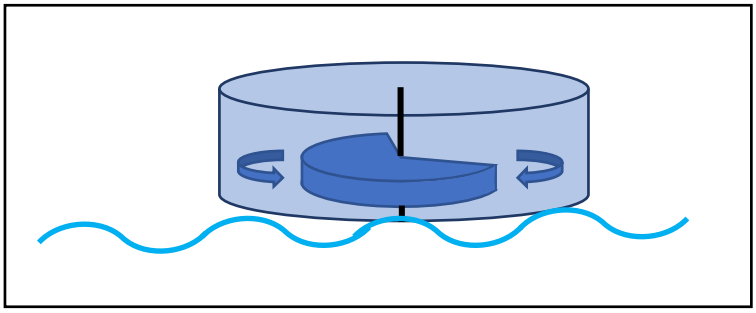

Figure 7: Concept rotating mass.

1.4 Research on Point Absorbers from Uppsala University

Uppsala University developed a WEC based on the point absorber concept (see concept No. 1 in Figure 1). The Seabased Group commercialised and refined this idea. A buoy, commonly called point absorber, floated on the water surface and moved up and down with the wave motion. On the seabed, a linear generator was placed and connected with a rope to the buoy. The "rotor" was in this case a magnetised piston that moved up and down in the stator construction which was fixed to the seabed and was the foundation for the coil windings. Due to the vertical movement of the waves, the piston was moved up and down in the stator and generated a varying magnetic flux. Due to the reciprocal motion of the translator, the voltage delivered by the WEC needed to be transformed by power electronics in frequency and amplitude. This electricity can then be fed into the grid. More details about the design and development of the point absorber concept can be found in (1, 14–18).

The stator current can be controlled actively which improves the power output of a point absorber by reducing losses and enhancing power quality. (19) gives a closer look on the different alternatives of controls. The input for one of the systems was the speed (20) and the position of the point absorber. (19, 20) Therefore, it will be important to be able to track the motion of a point absorber buoy accurately.

A research group of Uppsala University already developed in (21) such a system that measured the movement of a buoy in the water in the test field of Uppsala at Lysekil, Sweden. The measurement in (13) was carried out by a buoy equipped with an accelerometer, a pitch/roll velocity measurement device and a force transducer. (21) During the evaluation it became clear that it was difficult to match the information. Also, a drift in the data could be observed. (21) As a future outcome it was recommended to merge information from different sensors or measurement systems by integrating a clock. (21)

Lysekil is located on the west coast of Sweden between Gothenburg and the border to Norway. Here, the sea can differ between a calm sea and high and powerful waves. Referring to site No. 9 in (22), the highest significant wave height that was measured over the past 8 years was 3,8 m whereas the waves during summer were low. On the 5th June 2020 however the wave heights were only between 0,28 and 0,48m high. (23)

1.5 Research Question

This thesis project focusses on the development and construction of a measurement system that should be able to track the motion of a buoy also for the test area in Lysekil, Sweden. It should be accurate and able to avoid the data merging problem of (21) . This system can help to provide the information of the position and movement of a point absorber for the implementation of an active control in this WEC as described above.

Some basic information was collected earlier through pre-studies during the Sixth Workshop for Maritime Technologies at the Sven Lovén Centre (July 1st to July 5th, 2019). (24) There, a small measurement system installed in a buoy was built and tested. (24, 25) In general, it could be evaluated that a solar-battery combination could supply the electronics in the buoy and that the used transmission system was too weak to reach the expected range over the water surface, in this case saltwater. (25) This pre-studies were realised under the supervision of Irina Temiz, Uppsala University.

The project is split into three different parts (Figure 8 shows an overview):

- Measurement system:

  For this part of the project, a suitable sensor technology needs to be evaluated. Then, a precise and accurate sensor unit has to be found and implemented into the system on the buoy. Therefore, different sensors that are already available on the market should be compared and the most precise one should be chosen. The sensor should be able to evaluate all the possible motions of a buoy in the water. The measurement system itself consists of sensors, a microcontroller and a possible data storage.

  In addition to that it is decided that the project should be extended. In the future the buoy should be able to measure the force that acts on it.

- Power supply:

  The system on the buoy needs to be powered. For this, a decision on the whole power supply concept has to be made: From the pre-studies (24, 25) it is known that it is possible to power the system with solar panels connected to a charge controller and a battery. The power supply design should be able to cover the requirements of the different components of all other parts of the project. As they will have a different voltage ranges, a suitable voltage level has to be evaluated. Also, the energy consumption of all system components must be taken into account.

- Data transmission:

  In (26), a study was made on an alternative communication system. Often, information is sent on the mobile network which can be a problem in more rural areas or development countries where the reception is not good or not available. A system could be evaluated that reached above land a 10 km range and that was able to send long commands.

  The task of this project is to implement and test this data transmission system. As a result, it should be evaluated if the system is able to handle the demands of this application.

This thesis includes the planning of the whole system, the main build-up of the circuit and the programming of the microcontroller. The implementation of the force transducer to the application and the build-up into the buoy will follow in a later state of the project.

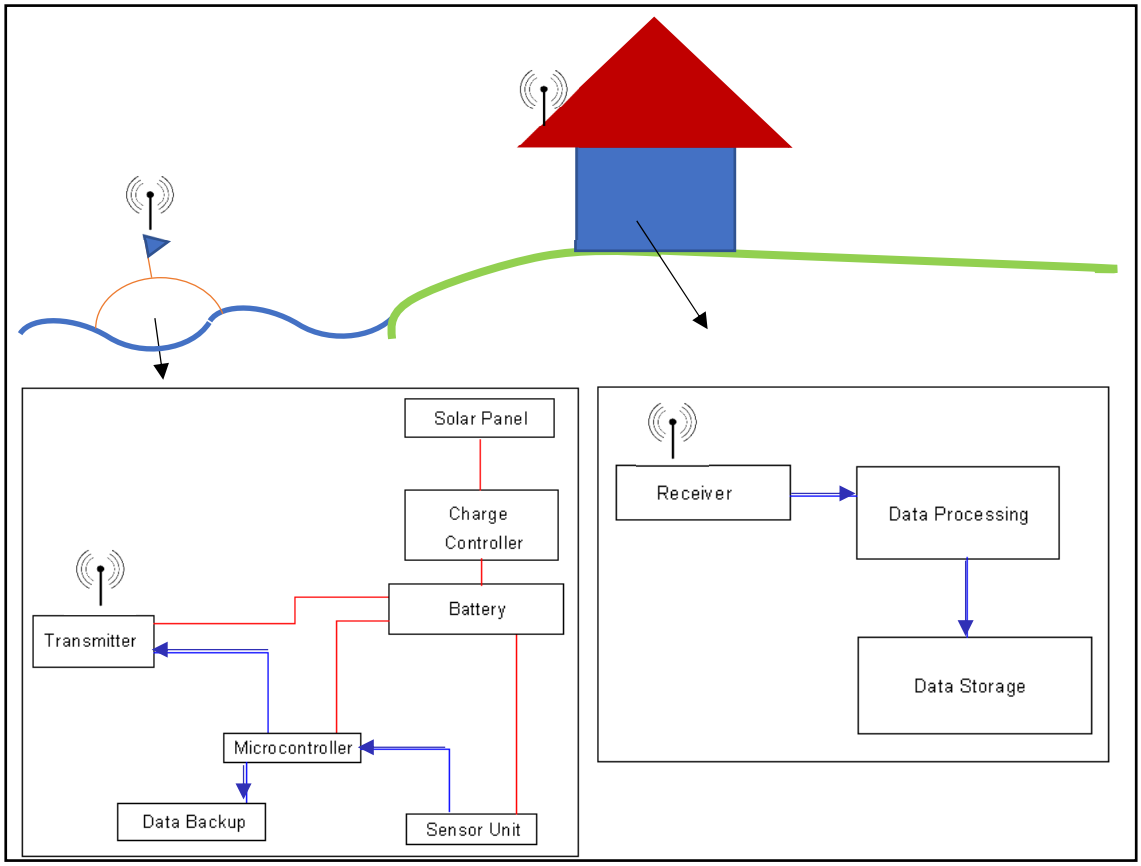

Figure 8: Project organization: Red lines denote the power flow and blue arrows denote the data exchange[4].

[4] Wireless symbol taken from: OpenClipart, freesvg.org, licensed under CC0 1.0 Universal (CC0 1.0) Public Domain Dedication, https://freesvg.org/wifi-icon-vector-image9255, cited: 05.06.2020

2 Theory and System Planning

This chapter describes the technical basics and functionalities of the utilised components and technologies. The preparational work, the choice of the measurement system and the dimensioning of the power system are also displayed. In addition to that, it contains the planning of the setup.

2.1 Six Degrees of Freedom

Note: The content of this chapter is based on (24, 25).

A buoy can move on all three spatial axes (X, Y and Z-axis (see Figure 9: X: "back and forward", Y: "right and left", Z: "up and down"). In marine applications the up and down movement is named "heave", the motion along the Y-axis "sway" and along the X-axis "surge". (27)

Around every of these three spatial axes turns can occur (roll, pitch and yaw (see Figure 9: roll: around X-axis, pitch: around Y-axis and yaw: around Z-axis)). (27) For this project especially the roll and pitch angles are interesting to track.

A sensor concept that is chosen for this application should be able to cover the straight movements on all three spatial axes and the turning angles around these (see Figure 9). This motion concept of taking into account all six different movements is called "six degrees of freedom" (DOF) as the buoy has the freedom to move in all these six dimensions.

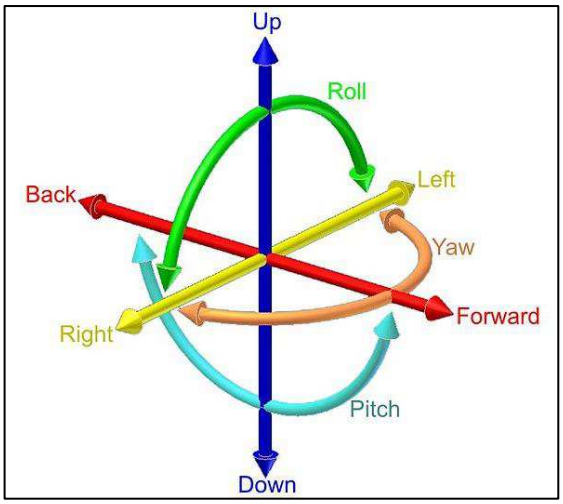

Figure 9: Six degrees of freedom[5].

[5] © Horia Ionescu, Wikimedia, licensed under public domain license, https://commons.wikimedia.org/wiki/File:6DOF_en.jpg cited 04.06.2020

2.2 Measurement System

This chapter shows different solution approaches and gives an overview about existing wave measurement buoy-concepts and their sensor technologies.

The first idea was a solution with ultrasonic sensors (see chapter 2.2.1). After more research in existing applications the usage of an inertial measurement unit (IMU) system proved to be the most reliable and accurate solution.

2.2.1 Ultrasonic Sensor

An ultrasonic sensor sends an ultrasonic sound pulse with a sound frequency higher than 20 kHz which is reflected from objects in the water or on the seabed. Both parts, the receiver and the transmitter, are placed together in one housing. The time between the emission of the sound pulse and the incoming echo is measured. With this time frame, the distance between the sensor and the object can be calculated. (28–30)

In coherence to the project:

The idea of an ultrasonic measurement is to attach four sensors around the buoy facing to the seafloor.

This measurement technology is good to use for only up-and-down-movements but as a wave never lifts the buoy just straight up and down, a tilting movement is always added to the movement. Due the tilting of the buoy, the sensors do not face in a straight direction to the sea floor (see Figure 10). Also, the seabed is innately not a straight surface due to for instance waves or the tides. This makes the interpretation of the distance difficult.

Another problem could occur if the sensor is sometimes lifted out of the water. Ultrasonic waves get partly reflected if there is a change of the materials they pass through due to a change of speed of sound (for example between air and water). (31) This leads to inaccurate measurements and results.

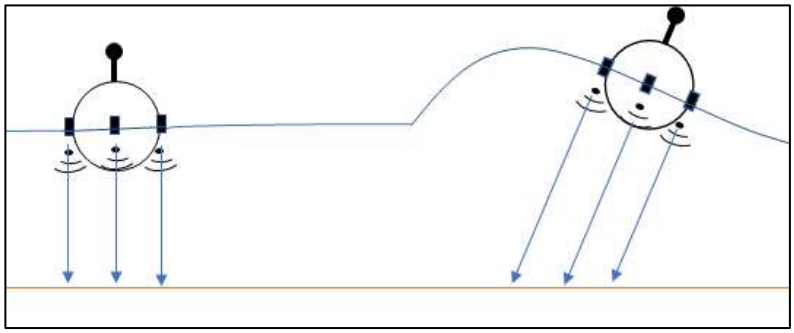

Figure 10: Tilted buoy with ultrasonic sensors.

2.2.2 Tracking with a Camera System

A camera is installed above a moving body in the water. It records the movement of the buoy and this is analysed to a motion profile. (32)

Some drawbacks are that there are disturbances due to water reflections and splashing water. Another disadvantage is that a fixed structure is needed to install the camera. (32)

2.2.3 Inertial Measurement Unit

(19) defines an inertial measurement unit (IMU) as a sensor unit that is able to track the movement of a body in directions of all three spatial axes.(33, 34) It needs to track in all three spatial axes to be able to cover all six DOF of the buoy movement (see Figure 9 and chapter 2.1). The used sensors are measuring acceleration (35) and rotation rate (35) in comparison to a reference frame, the commonly called Earth-centred inertial (ECI) reference frame (36).

An IMU consists of the sensors that measure acceleration and rotation rate in six DOF (see Figure 9) and an analogue-digital-converter (ADC) (34) which converts the incoming current- / voltage-signal into a digital format.

An IMU is a part of an attitude and heading reference system (AHRS) or an inertial navigation system (INS) which uses the sensor data for more information or further operations (see chapter 2.2.4). (36)

Sometimes the position is located due to the determination of magnetic fields (33) or by satellites (37).(33) If an IMU has a magnetometer implemented, it is often called nine-dimensional (9D) IMU (33). In addition to this, a positioning system can be included. Typically, these advanced IMUs are located in an AHRS or INS.

The IMU includes accelerometers and gyroscopes (and for 9D-modules also magnetometers) that measure all three spatial axes. Measuring the position related to magnetic fields helps to increase the accuracy of the measurement. (33)

2.2.4 Usage of an IMU in AHRS and INS

The IMU provides just the sensor data. This information is processed further in an AHRS or an INS. (36)

An AHRS is used for example in remotely operated underwater vehicles (ROV) and can provide positioning in real-time. (38) In addition to the IMU it has a digital processing unit (38) which links the different raw data together and calculates also the heave as roll and pitch angles. (37–39) Mostly, an extended Kalman filter is included into the system which helps to separate the sensor signals from noises (40) and to support the optimisation of the estimation algorithm that calculates the relative position. (41, 42)

An INS takes also the velocity into account and can estimate the position compared to a start point over time. Positioning with global navigation satellite system (GNSS) (see chapter 2.3.4) prevents the relative position from drifting away. (43)

2.2.5 Available Systems on the Market

Most of the buoys that are available on the market work with an IMU system like AHRS or INS because it has the possibility to be more accurate and reliable: due to the fusion of different sensor data and the usage of the Kalman model.

With this information, the further focus is set on these technologies. To evaluate the best system for this project a comparison is made between different devices.

In Table 1 different sensors are listed which are used for measurement buoy applications or which are taken into account:

Table 1: Different sensors in measurement buoy applications.

Sensor	Application	Heading accuracy [°]	Roll/Pitch accuracy [°]	Heave accuracy [cm]
Aanderaa MOTUS Wave Sensor (44, 45)	Datawell Waverider, EMM2.0 Coastal Buoy, etc.	-[6]	-	5
IG-500A / Ellipse-A miniature AHRS (46)	Wave buoys in the Arctic sea Ice (46)	0,8	0,2	10
Crossbow CXL02LF2Z vertical accelerometer (±2G)	Wave buoy measurements at the Antarctic sea ice edge (47)	-	-	-
Spotter Motion Sensor (48)	Spotter V2 buoy (49)	-	-	2
MTi-G-710 GNSS/INS (50)	No example	0,8	0,2	-
LT-500 AHRS (51)	No example	1,5	0,5	-
Ellipse2-D (37)	**Chosen sensor for project buoy**	**0,2**	**0,1**	**5**

The Ellipse2-D AHRS/INS is highlighted as a very accurate system compared to the other considered opportunities. Solely the Spotter Motion Sensor promises a better heave accuracy but this sensor is only available in combination with the Spotter V2 buoy and is not sold individually. As a consequence, it is not qualified for this project.

The Ellipse2-D is also equipped with a magnetometer and a GNSS system to supply the project with heading information. (37) It can be used as an AHRS and INS, so it could also be used for navigation solutions as it provides matched motion profiles depending on the application. (37) Due to the combination of AHRS and INS, the Ellipse2-D uses the dual antenna GNSS positioning to improve the calculations of the relative position and gains a better precision compared to the other Ellipse sensor units. (37)

2.2.6 Real Time Kinematic

During the project it is discussed if the system can be improved with a real time kinematic (RTK) implementation. It helps to improve the accuracy of the GNSS. Therefore, a static transmitter is needed in the surroundings. There are two possibilities, either to buy a license from an RTK-provider or to set up an independent system.

In this case, an RTK-feedback improves the heave accuracy from 5 to 4 cm which is a low improvement compared to a high technical complexity as it needs a real-time feedback loop to the Ellipse2-D and economical expenses.

Because of these drawbacks, the RTK system is not further considered.

[6] For this particular information was no data available

2.3 Applied Sensors Concepts

The functional principles of the applied sensors are explained in this chapter.

For this project, the Ellipse2-D sensor system of SBG Systems is used which includes a three-axis accelerometer and gyroscope, a magnetometer and a satellite positioning system. It also contains a Kalman-filter to convert the raw data into heave in meter or turning angles in degree.

In a later state of the project, a force transducer shall be included in addition to the Ellipse2-D, therefore also the working principle of it are outlined here.

2.3.1 Accelerometer

Note: The content of this chapter is based on (24, 25).

The change of movement of an object in one direction can be sensed by an accelerometer. (52–54) For this project the accelerometer concept of a micro electro mechanical system (MEMS) is important to understand and is explained in this chapter. MEMS are small sensor concepts and are applied for example in smartphones and driving assistance systems. (53, 55) In larger installations the piezo-electric effect is used. (56)

To understand how the MEMS accelerometer-concept works a closer look into the setup needs to be made:

The accelerometer consists of:

- the mechanical part: a comb-structure that has an agile mass (marked blue in Figure 11) and a fixed part (marked black in Figure 11) which are connected with each other with strain gauges or springs (52–54)
- an electronical part: this part helps to convert the output of the mechanical part into an electrical output (depending if the sensor has a current or voltage output) (52–54)

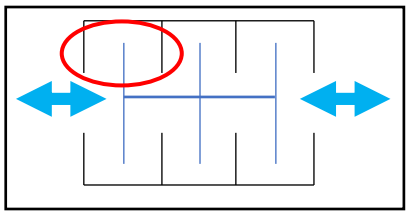

Figure 11: Comb structure – accelerometer.

Figure 12 shows a more detailed view into the red marked section from Figure 11: the agile plate is connected on both sides via springs to the fixed plates. Two plates together form a capacitor. (53)

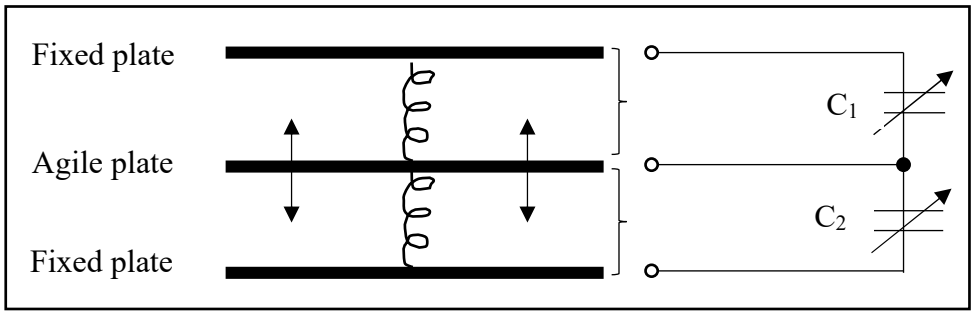

Figure 12: Equivalent circuit diagram: basic concept of a MEMS-accelerometer (25).

Due to a change of motion, the agile structure is pushed in the other direction and starts to move to one side of the comb the capacitance is changed and measured. These values are converted by the electronic part of the sensor and displayed as the sensor output (current or voltage) (see Figure 13). (53)

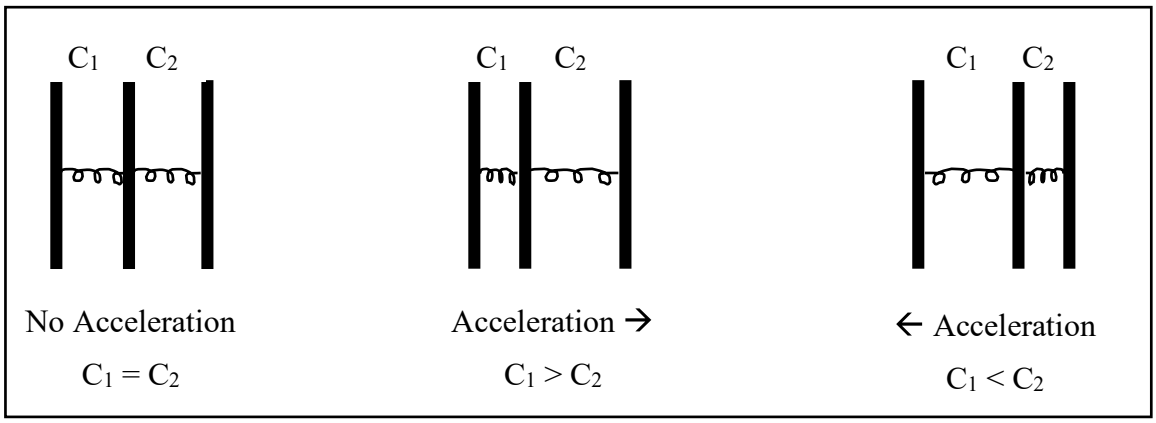

Figure 13: Sensor concept accelerometer – acceleration (25).

The acceleration always happens in the opposite direction of the agile comb motion (see Figure 13): This is comparable to the acceleration in a plane when the passengers are pushed into the seats during the start.

If strain gauges are used compared to springs, the compression or extension of them changes their resistances and this is measured and displayed. (54, 57)

2.3.2 Gyroscope

Note: The content of this chapter is based on (24, 25).

This chapter also focusses on the MEMS-application which is used for example in gadgets such as smart watches or safety systems. (55) A gyroscope senses angular movement in one axis by the usage of the Coriolis effect, especially motions like pitch, yaw and roll. (35, 58–60)

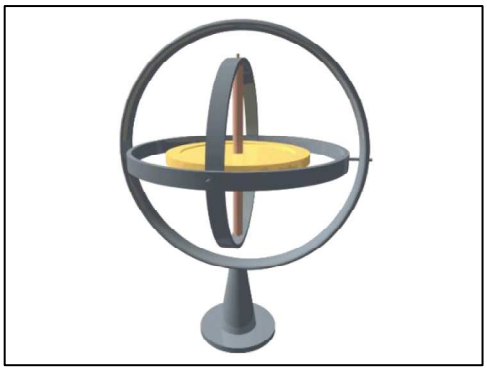

Figure 14: Gyroscope[7].

To increase the accuracy of the sensor, it normally consists of two identically constructed sensor parts that work vice versa, which means that the parts oscillate opposite in phase with each other. (61) Due to a rotational motion the Coriolis force acts on the different sensor parts in different directions and the capacitance $\Delta C \neq 0$. With linear motions, a force would act in the same directions on the two sensor parts and the capacitance $\Delta C = 0$. (35)

The set-up is related to the accelerometer concept out of chapter 2.3.1. First, there is a mechanical and an electrical part that converts the mechanical output of the sensor unit into an electrical (see chapter 2.3.1). (35, 61) The mechanical part in a gyroscope consists of three different frames that are nestled into each other and connected via springs (35, 61):

- The drive frame: A fixed frame that oscillates by an alternating current (AC) voltage forwards and backwards. (61)
- The Coriolis frame: This frame lays in between the drive frame and the detection frame and oscillates with the other parts. It is fixed to the other frames via springs. (61)
- The detection frame: This part is placed in the Coriolis frame and anchored to it via springs and consists of a comb structure that is similar to the accelerometer-structure shown in Figure 11. (61)

When the object moves in a straight line the detection frame is not moving. If the object is turning, the detection frame is deflected due to the acting Coriolis force on the Coriolis frame and the distances between the combs change. With this, a capacitance change can be detected (see Figure 12 and Figure 13). (35, 61)

[7] © Lucas Vieira, Wikimedia Commons, licensed under Public Domain License, https://commons.wikimedia.org/wiki/File:3D_Gyroscope-no_text.png, cited 22.05.2020

2.3.3 Magnetometer

A magnetometer senses magnetic fields, for example the magnetic field of the Earth (62) and detects the cardinal direction for devices such as smartphones as a digital compass. (63)

There are many different procedures how to measure a magnetic field, for instance: Hall effect, magneto resistive, anisotropic magneto resistive or giant magneto resistive. (64)

This chapter focuses on the measurement with the help of the Hall effect, the Hall sensor. The schematic is shown in Figure 15

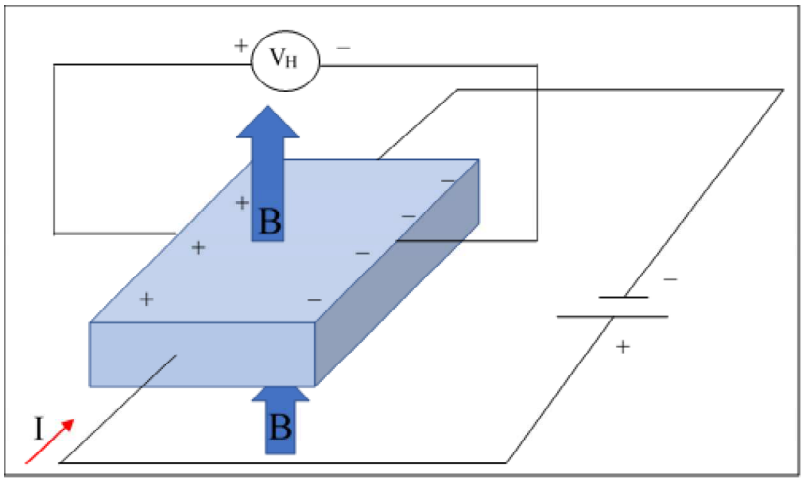

Figure 15: Hall sensor schematic.

Current flows through a Hall probe (conductor) (see Figure 16). (64–67)

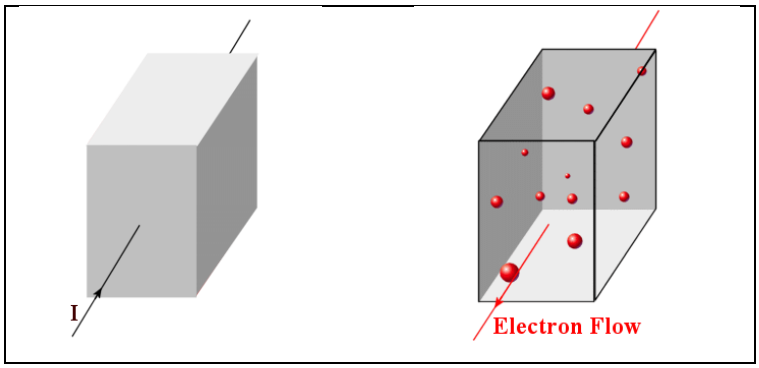

Figure 16: Hall effect – current flow[8].

If this conductor is placed in a magnetic field (67), the Lorentz force (left-hand-rule for the flow of electrons) is applied on the electrons which pushes them in a specific direction (see Figure 17). (64, 65, 68)

[8] © Blair Bonnett, Wikimedia, licensed under Creative Commons CC0 1.0 Universal Public Domain Dedication, https://upload.wikimedia.org/wikipedia/commons/2/23/Van_der_Pauw_Method_-_Hall_Effect.png, cited 20.05.2020

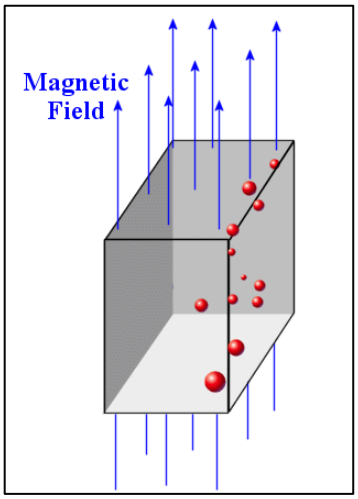

Figure 17: Hall effect – applied magnetic field[9].

An electric field (E-field) occurs in the Hall probe as the electrons are distributed unequally: in one side an excess of electrons (negatively charged) is created while the other side is positively charged due to a shortage of electrons (see Figure 18). (65, 68) This generates a measurable Hall voltage V_H. (65–68)

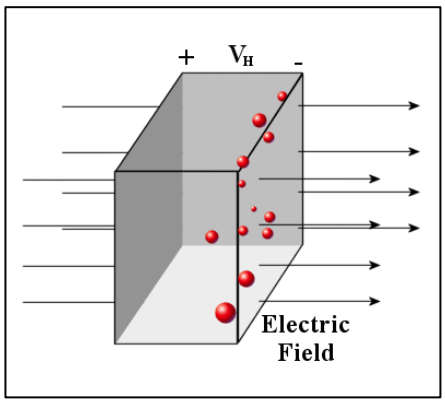

Figure 18: Hall effect – electric field[10].

The electric field applies a force F_{el} that tries to push the electrons back, against the applied Lorentz Force F_L. (65)

[9] © Blair Bonnett, Wikimedia, licensed under Creative Commons CC0 1.0 Universal Public Domain Dedication, https://upload.wikimedia.org/wikipedia/commons/2/23/Van_der_Pauw_Method_-_Hall_Effect.png, cited 20.05.2020

[10] © Blair Bonnett, Wikimedia, licensed under Creative Commons CC0 1.0 Universal Public Domain Dedication, https://upload.wikimedia.org/wikipedia/commons/2/23/Van_der_Pauw_Method_-_Hall_Effect.png, cited 20.05.2020

The electric field builds up until: (69)

$$F_{el} = F_L \qquad [1]$$

With this, the magnet field (B-field) can be calculated: (65, 67, 69)

$$E * q = B * v * q \qquad [2]$$

$$\frac{V_H}{d} = B * v \qquad [3]$$

With:

$$v = \frac{I}{n*e} \qquad [4]$$

$$B = \frac{V_H}{d*\frac{I}{n*e}} \qquad [5]$$

q: electrical charge

v: velocity of the charged particles

d: width of the Hall probe

I : current that flows through the Hall probe

n: density of the electrons

e: charge of the electrons

2.3.4 Global Navigation Satellite System

Note: The content of this chapter is based on (24, 25).

The global navigation satellite system (GNSS) is a system of satellites that orbits the Earth. (41) The receiver needs to be connected with to a minimum of four of those satellites simultaneously (70).

To increase the worldwide coverage GNSS includes different systems (see Table 2) (71–73):

Table 2: GNSS systems.

Name of the System	Provided by
Galileo	Europe
Navigational satellite timing and ranging – global positioning system (NAVSTAR GPS)	USA
Global'naya navigatsionnaya sputnikovaya sistema (GLONASS)	Russia
BeiDou navigation satellite system (BDS)	China

Every satellite sends continuously with the help of the radio signal the own position and the time $t_{satellite}$ of an atomic, synchronised clock. (41, 70, 73, 74)

If a receiver has a connection to one of the satellites, it directly receives the broadcast and connects the incoming message with a time stamp $t_{incoming\ message}$. (74)

As radio frequency travels by the speed of light (74) $c = 2{,}99 * 10^8$ m/s, the distance d between the receiver and the transmitter can be calculated by following equation: (74)

$$d = c * (t_{incoming\ message} - t_{satellite}) \qquad [6]$$

Now, the distance between the receiver and one satellite is known. With this knowledge, the satellite can be seen as a centre of a sphere with the radius of the distance d, while the position of the receiver is somewhere on the surface area. (41) (see Figure 19)

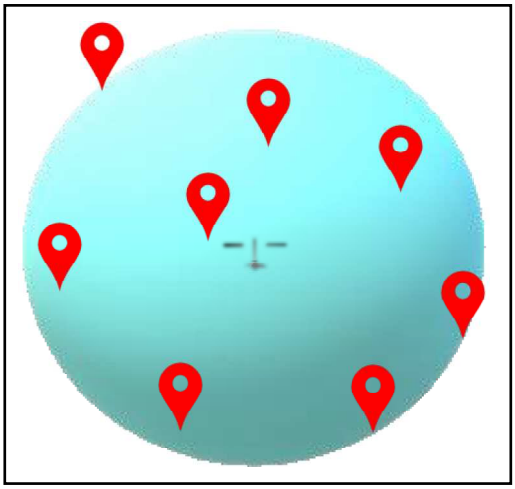

Figure 19: GPS positioning with one satellite[11] (25).

As every connection of the receiver to a satellite includes the position on a sphere around the satellite, with the connection to a second satellite, the position of the receiver can be limited to the circle of intersection between the two spheres. (41) (see Figure 20)

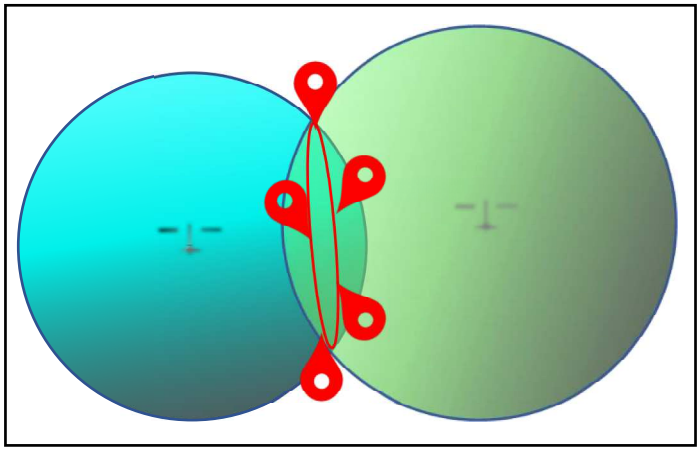

Figure 20: GPS positioning with two satellites[12] (25).

A third satellite is needed for an intersection between three spheres. Two possible locations are conceivable after considering this scenario: The point in space or inside the Earth can be neglected, as the receiver is situated on the Earth. (41, 42)

The fourth satellite provides an improvement of the positioning. (41, 42) The distances previously described are pseudo-ranges (41, 42, 70) because the clocks in the satellites are not

[11] Satellite taken from: © Piotr Siedlecki, Public Domain Pictures, licensed under CC0 Public Domain license, www.publicdomainpictures.net/se/view-image.php?image=250008&picture=svart-satellit, cited 05.05.2020 Position needle taken from: © Clker-Free-Vector-Images, Pixabay, licensed under Pixabay license, https://pixabay.com/vectors/location-poi-pin-marker-position-304467/, cited 05.05.2020

[12] Satellite taken from: © Piotr Siedlecki, Public Domain Pictures, licensed under CC0 Public Domain license, www.publicdomainpictures.net/se/view-image.php?image=250008&picture=svart-satellit, cited 05.05.2020 Position needle taken from: © Clker-Free-Vector-Images, Pixabay, licensed under Pixabay license, https://pixabay.com/vectors/location-poi-pin-marker-position-304467/, cited 05.05.2020

synchronised with the clock in the receiver. (42, 70) With the help of the fourth satellite, the offset between the fourth satellite and the receiver clock is known and with this, the offset to all of the satellites. This can be transferred to the other three time measurements and the pseudo-ranges become accurate distances. (41)

2.3.5 Kalman Filter

Sensor outputs are often influenced by noises, disturbances or temperature. Due to this, system outputs are often improved by the usage of filters, for example a Kalman filter.

Regarding to (75), a Kalman filter is defined as "a time series estimation algorithm". It is used mostly in real-time applications for unobservable values or to compensate observation errors. (75, 76)

The working principle is based on the combination of minimum two Gaussian functions. (77, 78) One example is a driving car. First, the initial position "position 0" of the car can be estimated by a GPS system and can be expressed as a Gaussian distribution as the position cannot be measured with a 100 % accuracy. Now, the car moves with a specific velocity. After some time, the new position "position 1" can be predicted by the knowledge of position 0 and for example the velocity (see blue line in Figure 21). Also, the GPS will measure a position 1 (see red orange line in Figure 21). Both principles that find a position 1 will be presented in Gaussian distributions. These are merged to a new Gaussian function which helps to increase the probability of the estimation of the relative position 1. (77–79)

The merged Gaussian distribution consist of:

- a merged Mean value (77, 79):

$$\mu_{merged} = \frac{\mu_1\sigma_2^2+\mu_2{\sigma_1}^2}{\sigma_1^2+{\sigma_2}^2} \quad [7]$$

- and a merged variance (77, 79):

$$\sigma^2_{merged} = \frac{\sigma_1^2{\sigma_2}^2}{\sigma_1^2+{\sigma_2}^2} \quad [8]$$

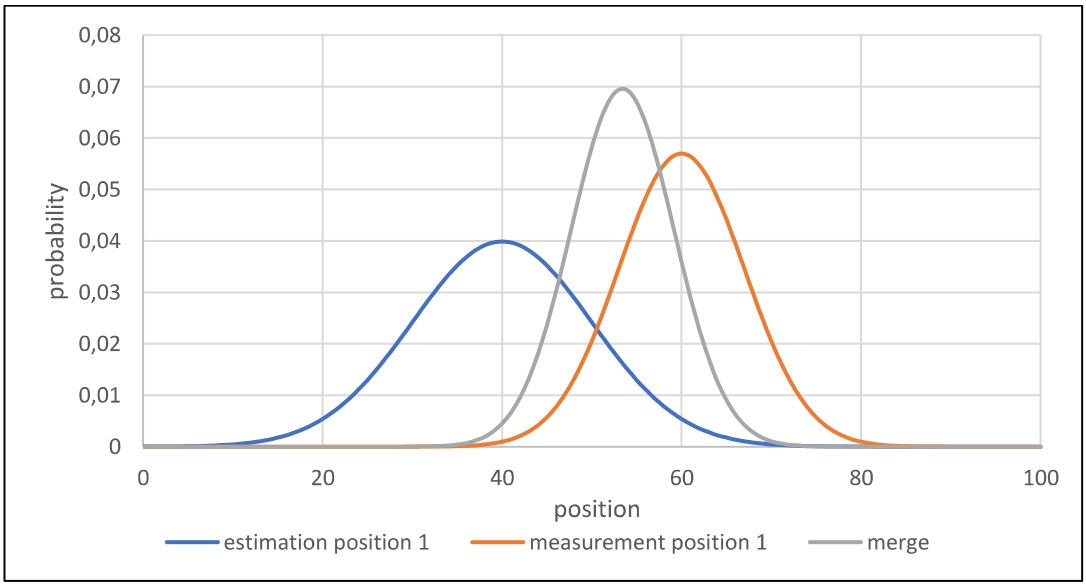

Figure 21: Kalman Filter in estimation of the position 1

2.3.6 Force Transducer

A force transducer measures the force or the weight that acts on the sensor (80) and detects tension and compression (81). It can be used to gather information on the maximum force that acts on a point absorber. Those data is necessary for example to be able to improve the fixing structure and the buoy material. (82)

Generally, a deformation measurement is made to obtain the forces that are acting on the object. (83) For this, following technologies are used: (83)

- < 0,1 µN: piezoelectric material
- < 25 µN: electrostatic or optical sensors
- mN-range: strain gauges

In the project, the strain gauges technology is used (80) and is described in this chapter. The Cambridge Dictionary defines strain as "a force or influence that stretches, pulls, or puts pressure on something […]" (84). (85, 86) A force of compression (negative strain ε) or tension (positive strain ε) (85, 86) acts on the strain gauges and changes their resistance proportionally to the strain (80, 85). (87, 88)

With this, the change of resistance can be calculated with the following equation (85, 88, 86):

$$\Delta R = R_0 * \varepsilon * k \qquad [9]$$

ΔR: change of resistance
R_0: basis resistance of the strain gauge without an extra acting force on the strain gauge
ε: strain
k: sensitivity factor, also called gauge factor (85, 86)

This formula shows that:

- compression decreases the resistance (88) and
- tension increases the resistance (88)

Usage of the effect for the sensor:

The change of resistance is measured in the sensor application. (87) The strain gauges are attached to the sensor housing (80, 83) and are connected in one of the layouts of a Wheatstone bridge, where either one, two or four (80) of the shown resistors in Figure 22 are replaced with a strain gauge (see Table 3) (85, 86).

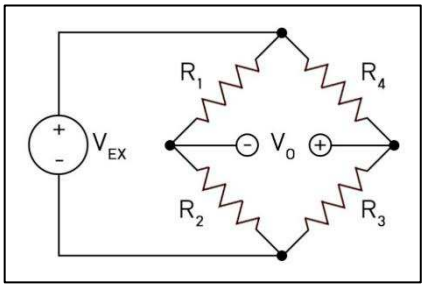

Figure 22: Wheatstone bridge circuit[13].

Table 3: Layouts of a Wheatstone bridge.

Set-up	Amount of strain gauges
Wheatstone full bridge	4
Wheatstone half bridge	2
Wheatstone quarter bridge	1

A usage of precision monitors is needed at constellations like the Wheatstone half bridge and Wheatstone quarter bridge (80), while the Wheatstone full bridge shows the best sensitivity (85, 86).

In idle state (no force is acting on the strain gauges), the output voltage V_0 of the Wheatstone bridge is zero, the bridge is balanced. (85, 86)

The output voltage can be calculated by following equation (85, 86):

$$V_0 = \left(\frac{R_3}{R_3+R_4} - \frac{R_2}{R_1+R_2}\right) * V_{EX} \qquad [10]$$

Due to an acting force the bridge is unbalanced and $V_0 \neq 0$.

In the end, the strain ε can be calculated out of the voltage ratio (86): [14]

$$\varepsilon = -\frac{V_{ratio}}{k} \qquad [11]$$

With (86):

$$V_{ratio} = \frac{V_{0\,(with\ force)} - V_{0\,(idle\ state)}}{V_{EX}} \qquad [12]$$

[13] © Daraceleste, Wikimedia, licensed under the Creative Commons Attribution-Share Alike 4.0 International license, https://upload.wikimedia.org/wikipedia/commons/5/5b/Wheatstone_bridge.jpg, cited 20.04.2020, taken without changes

[14] This formula is just valid only for the set-up of bending strain calculation (also not for Poisson strain calculation)

2.4 Power Supply

This chapter relates to the dimensioning of the power supply system.

In the end, the power supply shall be a system consisting of four solar panels, attached to a steel structure on top of the buoy. They are connected to a battery through a charge controller which controls the charging and discharging processes of the battery.

For the first test until the buoy and its accessories will be delivered, a smaller scaled system is implemented.

2.4.1 Battery Dimensioning

Voltage Level

To supply the measurement system, a voltage level needs to be set for all the components (see Table 4):

Table 4: Voltage ranges for the different components.

Component	Voltage Range [V]	Supplied by
Arduino Mega 2560 (89)	recommended: 7 - 12 limit: 6 - 20	Battery through 12 V voltage regulator
Ellipse2-D (37)	9 - 36	Battery
Adeunis RF ARF7940BA (90)	4,5 - 36	Battery
Force Transducer DDENA2H (80)	8,5- 28	Battery
MAX232 (91)	5	Arduino 5 V Pin
SD-card shield (92)	5	Arduino 5 V Pin

The choice to set the system voltage of this project on 12 V is due to:

- All components can be supplied with 12 V (see Table 4)
- In the pre-study project the system was already supplied by a 12 V battery (24, 25)
- The charge controller from the pre-study project (24, 25) can be reused

Energy Consumption and Battery Dimensioning

To calculate the size of the battery it is important to calculate the maximum possible power consumption of all the system components (see Table 5) because this defines the minimum time that the system can last without being recharged.

Table 5: Calculation of the maximum energy consumption.

Component	Max. Power [mW]	Expected Working Hours [h]	Max. Energy Usage [Wh/day]
Ellipse2-D (37)	1 500	24	36
Arduino Mega 2560[15]	4 000	24	96
Adeunis RF ARF7940BA (90)	500	24	12
Force Transducer DDENA2H[16]	264	24	6,34
Sum of the max. energy consumption in Wh/day:			∑ 150,34

The maximal energy consumption regarding Table 5 adds up to ca. 150 Wh/day, divided by the 12 V battery voltage results in 12,5 Ah for 24 hours. With a minimal survival time of ca. 48 hours without charging, the battery should have a capacity of at least 25 Ah. The applied battery for the first tests covers 30 Ah.

Since the expectation of the power consumption is lower than above, the survival time increases: The measured current is 370 mA without the force transducer (see Figure 23), which implements a power of ca. 4,5 W, giving an energy consumption of about 108 Wh/day and a needed capacity for 24 hours of approximately 9 Ah. This implies an energy security buffer of about 3,3 days without charging.

The charge controller indicates with a light-emitting diode (LED) that the battery charges even with low sun irradiation. This also increases the time of energy security.

The battery in the end application will be 60 Ah and 12 V. This means that the battery could last for approximately 6,7 days without sun light which improves the energy security, especially for the winter time significantly.

[15] The Arduino microcontroller runs with 5 V and maximum 800 mA. (85) With this, the maximal power consumption will be 4 W.

[16] The force transducer DDENA2H will work with the 12 V battery-system. The typical operating current for an ICA2H system is 22 mA. (86)

2.4.2 Solar Panel

Now, it is explained how the solar cell is chosen. As the buoy is placed in Sweden the peak sun hours vary a lot between summer and winter. The first test takes place during summer 2020 before the buoy will be delivered with the final solar panels. Because of that, a small solar module needs to be chosen.

At the coast, the sun radiation over a year is in average ca. 1000 kWh/m². (93)

Following assumptions are made:

- There is no shadowing due to the seaside location
- It is estimated an average time of peak sun hours per day of about 2 hours during winter (which points out to be the worst case scenario for solar energy) and around 7-8 hours during summer (94)
- 9 Ah capacity and a daily energy use of 108 Wh (see chapter 2.4.1)

Required peak power of the solar panel during winter (solar panel dimensioning for the end application): (95)

$$\frac{Daily\ energy\ use}{Peak\ sun\ hours} = \frac{108\ Wh}{2\ h} = 54\ W_{peak} \quad [13]$$

And during summer: (95)

$$\frac{108\ Wh}{7\ h} = 15{,}5\ W_{peak} \quad [14]$$

With this, a solar panel for the testing in the summer 2020 of minimum 16 W_{peak} is needed.

For the end application the solar panels should not be scaled beyond 55 W_{peak}.

As the final location is on the sea and the motion of the buoy is uncontrollable following points also have to be considered:

- saltwater-proof
- The implementation of minimum two solar panels to secure a higher probability of getting direct incoming light as the facing direction is not controllable

There are also different materials on the market available (see Table 6): (95)

Table 6: Comparison between different solar cell materials (95).

	Monocrystalline	**Polycrystalline**	**Thin Film**	**Multi-junction**
Price	More expensive	Cheaper	Cheapest	High
Efficiency	15-22 %	13-15 %	14,7 %	Highest Record: ~46 %

Multi-junction solar cells are mostly used for military or space applications. (95) Due to the high price they are not considered for this project.

The higher the efficiency the smaller the solar cell. (95) This means that in the other three cases, monocrystalline would need less space for the same power than a panel that uses the thin-film technology. The area is important to consider on a small buoy.

In general, there are not many solar cells explicit marked as salt-waterproof what makes it difficult due to a reduced selection. The choice is made between following solar modules (see Table 7):

Table 7: Collection of different modules.

	CT30 SolarMarine[17]	SunWare 20164[18]	SunWare 20163[19]
Nominal power (W_p)	30	38	25
Nominal voltage (V)	12	12	12
Length (mm)	665	599	481
Width (mm)	342	481	426
Weight (kg)	1,4	1,8	1,7
Material	polycrystalline	polycrystalline	polycrystalline

In the end, the decision is made on the SunWare 20163 due to the size.

2.4.3 Charge Controller

To protect the battery from overcharging in an off-grid system, a charge controller should be added into the solar-battery-system between the photovoltaic (PV) and the battery. (96–98) Charge controller work either with the pulse width modulation (PWM) or the maximum power point tracking (MPPT) method. (98)

Main functions of a charge controller are:

- To interrupt current flow between battery and PV-system once there is no sun energy (97)
- To interrupt current flow between battery and PV-system if battery is fully charged (96, 97)
- To interrupt power supply to the load when the battery is empty or the load consumes too much power (96)

As the battery voltage has not changed from the pre-study project, the LS1024EU charge controller is reused. This charge controller follows the PWM principle which is explained further in this chapter.

A PWM charge controller has a switch between the PV and the battery. This switch can be controlled in switching frequency and duty cycle. (97, 98)

[17] https://www.elfa.se/Web/Downloads/_t/ds/CTsolarmarine_eng_tds.pdf?pid=11035175

[18] https://www.conrad.se/p/sunware-20164-polykristallin-solpanel-38-wp-12-v-1456325

[19] https://www.conrad.se/p/sunware-20163-polykristallin-solpanel-25-wp-12-v-1456324

At the start, the charging voltage of the battery is applied including some extra voltage to compensate losses. (99) As soon as the battery gets charged, the battery voltage increases and with this the applied charging voltage. (99) Normally, the switch is constantly open until a (from the company pre-defined) state of charge (SOC) is reached. (97–99) This can be detected by measuring the battery voltage. (97–99) After this, the charging current is slowly reduced by using the switch. (97) The switching process continues to avoid overcharging and at the same time prevents a loss of the SOC. (97, 99)

2.5 Data Transmission

This part of the project follows the projects that are described in (24–26). This chapter just defines some different aspects of data transmission. For a more detailed theory research – please have a look at the project work (26).

In the project an 868 MHz radio transmission system is used. This chapter focuses on this part of transmission systems.

868 MHz belongs to the ultra-high frequency (UHF) range (100) and to the radio frequency (RF) which has a frequency range from 3 kHz up to 300 GHz (101).

(101) defines radio frequency electromagnetic radiation as "the transfer of energy by radio waves" which is present in following applications: "[r]adio and television broadcasting, mobile phones, wireless networks such as [Wireless Fidelity (Wi-Fi)], cordless phones, police and fire department radios, point-to-point links and satellite communications" (101).

Due to the modulation of the signal, as for example amplitude modulation (AM) or frequency modulation (FM), information can be sent via radio waves. (102) During the AM, the amplitude of the carrier wave is changed while the phase and the frequency stay constant. (102–104) During FM the frequency is varied while the other parameters of the carrier wave does not change. (102–104) Other signal modulation techniques are for example the phase modulation, the pulse-width-modulation, the amplitude or frequency shift keying.

FM is less failure-prone because the amplitude is more sensitive for disturbances. (104)

For example: If the data that should be sent is a binary number (that means it just contains "0" and "1"), the AM and FM would differ as described in Table 8 (102). Every full wave gives one character. (102)

Table 8: AM / FM example (102).

	AM	FM
Amplitude	Low amplitude to send a "0" High amplitude to send a "1"	Constant
Frequency	Constant	High frequency to send a "0" Low frequency to send a "1"
Phase	Constant	Constant

3 Method

3.1 Power Supply

To test the system before the buoy and its onboard battery and solar panels are delivered, a solar panel and a battery are added to the system. Those will not be included in the final application. The battery voltage will remain at 12 V.

3.1.1 Connection of the Components

The circuit[20] is first tested with a voltage source with current control to avoid damage to the components. The measured current is approximately 320 mA (370 mA with data transmission process). With this information for the power supply application with battery (see Figure 23), a 2 A fuse is added (to replace the current control) into the circuit for protection.

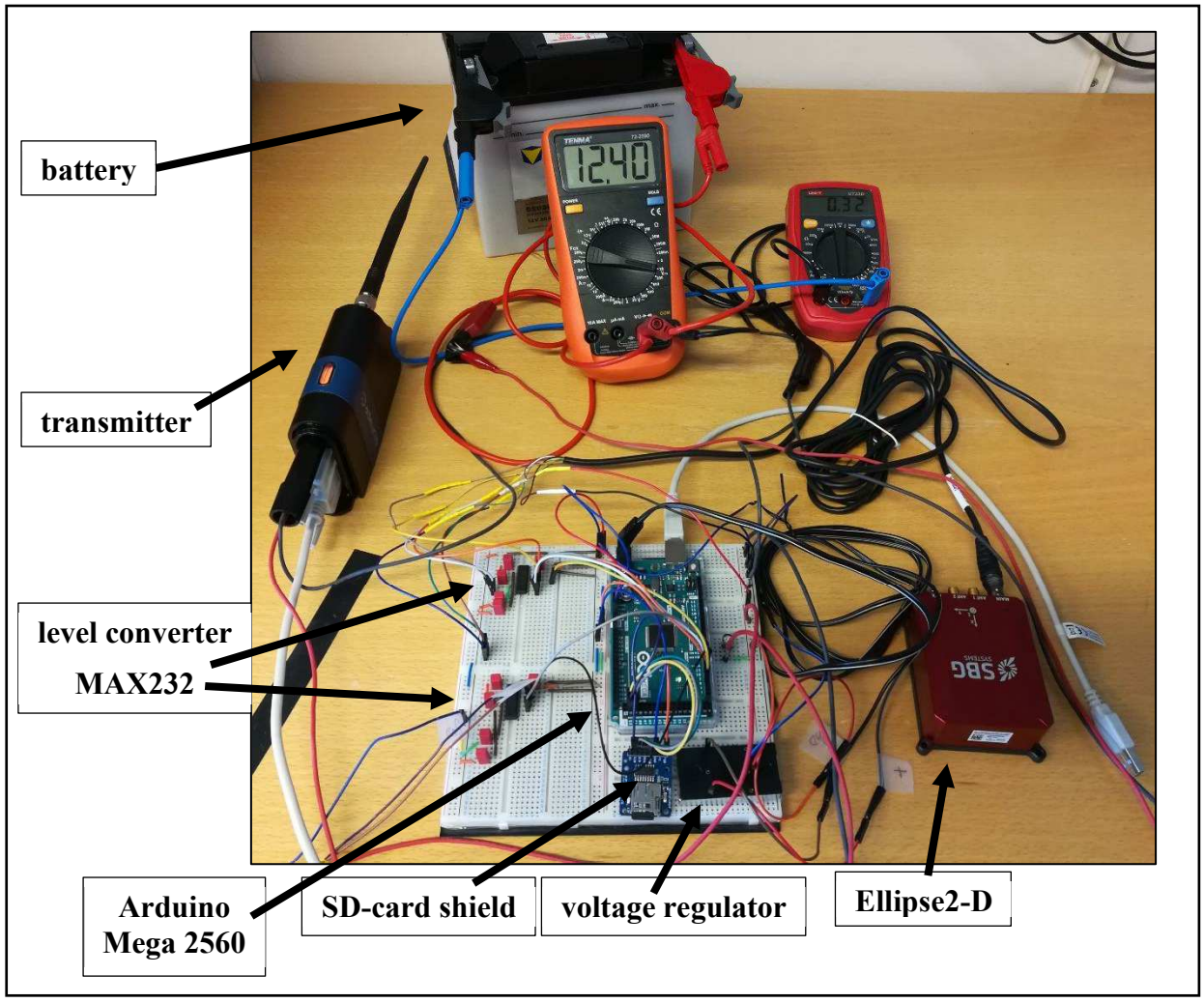

Figure 23: Connected circuit to the battery.

[20] Including the Arduino, the two MAX232 ICs, the Adeunis transmitter, the Ellipse2-D, the SD-card shield

The voltage supply cables (red and black, see Table 9) that come from the Ellipse2-D need to be connected to the 12 V battery voltage (see Figure 25).

The force transducer with the ICA2H system works with a voltage range between 8,5 V to 28 V (105) and can also be connected to the battery voltage in a later state of the project.

The Arduino Mega 2560 has a recommended voltage range from 7 to 12 V. (89) As the battery voltage depends on the SOC, it can exceed 12 V (see Figure 24). To avoid extra stress on the onboard voltage regulator, a DC/DC (DC = direct current) converter is added to the circuit (see Figure 25). This allows an input voltage range from 9 V to 18 V with 830 mA and provides a stable output voltage of 12 V. This is supplied by the power jack connector.

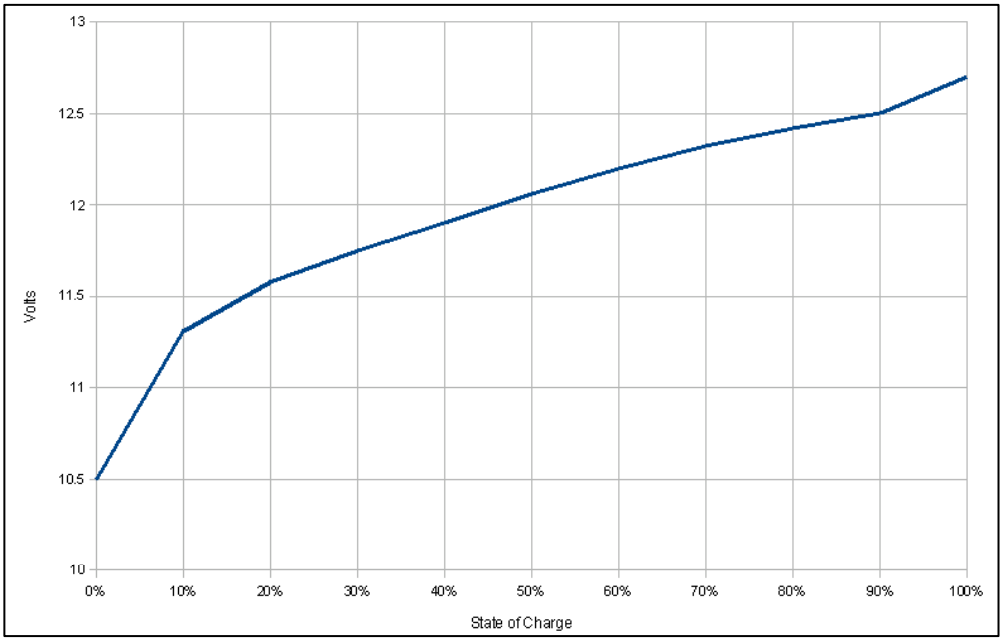

Figure 24: SOC [%] versus the battery voltage of a lead-acid battery[21].

The MAX232 level converter and the secure digital memory card (SD-card) shield need an input voltage of 5 V and is powered by the 5 V pin of the Arduino. (see Figure 25)

[21] © Mikiemike, Wikimedia Commons, licensed Public Domain license, https://upload.wikimedia.org/wikipedia/commons/7/79/Lead-acid_voltage_vs_SOC.PNG, cited 31.05.2020

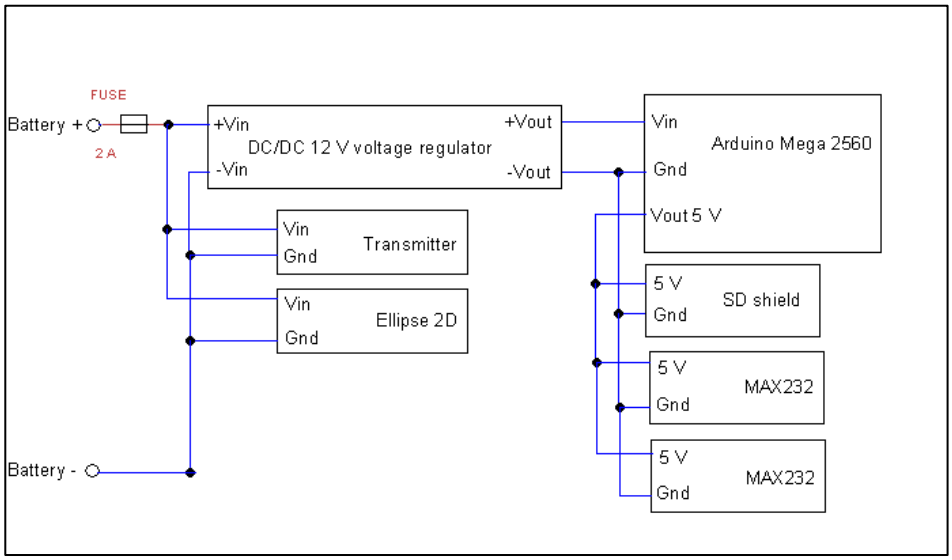

Figure 25: Power supply circuit.

3.1.2 Connection to the Power Supply

Note: These descriptions are taken from (106).

Figure 26 and Figure 27 show how the circuit and the battery are linked to the charge controller: To protect the battery, a 5 A fuse is added to its plus pole.

Then the battery is coupled to enable the charge controller to adjust its settings regarding the 12 V battery.

Afterwards, the solar panel is connected. To prevent the system from sparks, the panel should be covered during the connection process.

Finally, the load is included. Therefore, the load should be switched off.

At the end, the charge controller needs to be set to the right type of battery. Therefore, the button is pressed for approximately five seconds:

- One LED: sealed battery
- Two LEDs: gel battery
- Three LEDs: flooded battery.

The battery that is used for this state of the project is a flooded battery (setting 3).

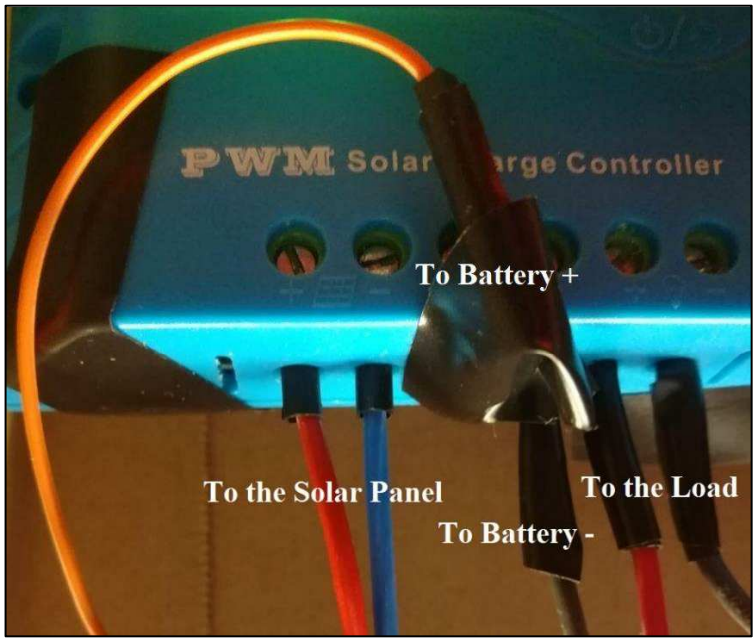

Figure 26: Connection to the charge controller.

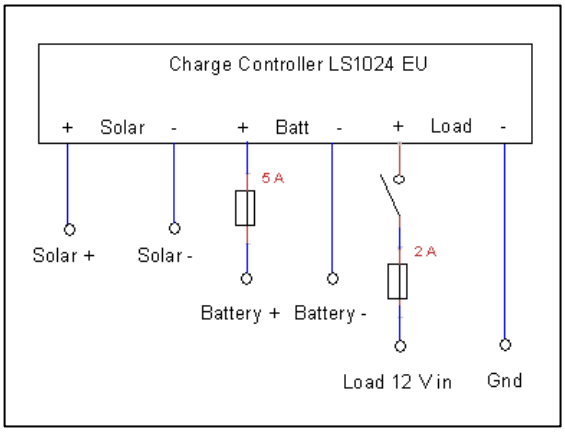

Figure 27: Circuit around the charge controller.

3.1.3 Testing

The power supply system is tested in two different steps:

- Replacing the voltage source with current control with the battery in the laboratory
- Checking the system in a 48 hours test: let the whole connected system including the solar panel, the battery, the charge controller and the load that is switched on run over 48 hours and compare the SOC of the battery between the start and the end of the test.

3.2 Measurement

This chapter shows everything with respect to the sensor unit:

- Which basic settings does the sensor system need?
- How does the Arduino pick up the data?
- How can the information be stored on the SD-card?

3.2.1 First Preparations

USB Cable Driver Configuration (107):

At the start some basic settings need to be adjusted. For this, the Ellipse2-D is connected via the RS232/universal serial bus (USB) cable to the computer and the software "sbgCenter Application" that is delivered together with the sensor. The USB cable driver configuration (107) helps to ensure a working connection between the sensor and the computer: According to the manual, in the port settings of the device manager, the latency timer needs to be set to 1 ms and the serial enumerator to be unchecked. (107)

General Settings in the sbgCenter Application:

In the sbgCenter Application the baud rate and output mode need to be changed: The output mode has to be set to RS232, as the Arduino Mega 2560 uses this interface to connect to the Ellipse2-D. The baud rate must be set to 115.200 baud, since this is the maximal possible rate of the used level converter unit.

In the next step, the selected Kalman filter option is adjusted for the application by selecting the "Marine" model.

To choose the output message, Ellipse2-D supports the usage of National Marine Electronics Association (NMEA) messages. (39) These are standardised for marine and navigation communication applications and express different data in a text line. (108) They are in a pre-set format.

The Ellipse2-D is able to deliver data on two ports that can be adjusted to the needs of the application:

- Port A shall provide the results of the Kalman-model in the end which is possible with the NMEA message "PASHR". This ensures availability of the heave in meter, the coordinated universal time (UTC), and the roll and pitch turnings in degree. The "PASHR" output is set to a 5 Hz frequency.
- Port E however shall give the raw data from the sensors and the date. For the date information, the NMEA- "ZDA" message with a frequency of 1 Hz is used. The "PSBGI" message from NMEA delivers the UTC and the read data also in a 5 Hz frequency from the accelerometer in m/s^2 and the gyroscope in °/s for all six DOF.

To be able to split in an easy way the raw data and the calculated sensor values delivered by the Kalman filter, both ports, port A and E, need to be enabled in RS-232 mode.

3.2.2 Gather the Data from the Ellipse2-D

To connect the Ellipse2-D-RS232-interface to the Arduino, a level converter is needed. The chosen component is the MAX232. It helps to put down the incoming RS232 voltage levels of about +/- 12 V to 5 V transistor-transistor-logic (TTL) / complementary metal–oxide–semiconductor (CMOS) levels (91) which is necessary for the Arduino and vice versa.

Figure 28 and Figure 29 show the connection (91) from the sensor to the Arduino through the MAX232. Serial port 1 collects the information from port A from the sensor unit whereas serial port 2 is responsible for the data traffic from port E.

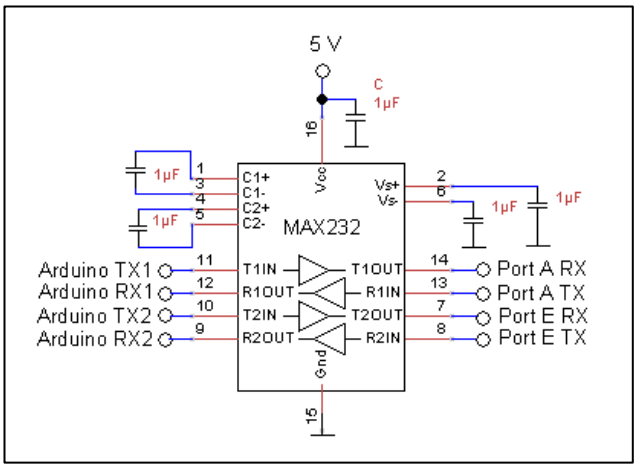

Figure 28: Connection of the integrated circuit (IC) MAX232.

Table 9 (109) shows how the cable of the Ellipse2-D are connected to the circuit:

Table 9: Connection of the Ellipse2-D.

Colour	Ellipse2-D Signal	Connected to
Green	SYNC IN A – ODO B	---
Blue	SYNC IN B – PORT B RX ODO A	---
Red	VIN	Battery +
Black	GND	Battery -
Brown	SYNC OUT A	---
White	PORT E TX	MAX232, R2in, Pin 8
Yellow	PORT A TX	MAX232, R1in, Pin 13
Orange	PORT A RX	MAX232, T1out, Pin 14
Grey	PORT E RX	MAX232, T2out, Pin 7

From the hardware manual (109) it can be seen that the green, blue and brown cable are not needed until this point of the project. They can be used to synchronise other sensors with the Ellipse2-D.

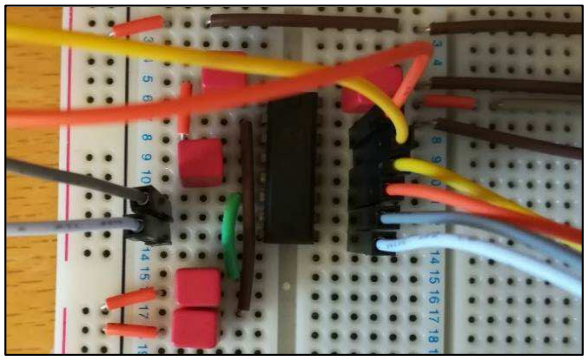

Figure 29: Connected MAX232 IC to the Ellipse2-D.

To be able to process the data from the Ellipse2-D, they have to be picked up from the Arduino. Figure 30 demonstrates the process flow of this part of the process:

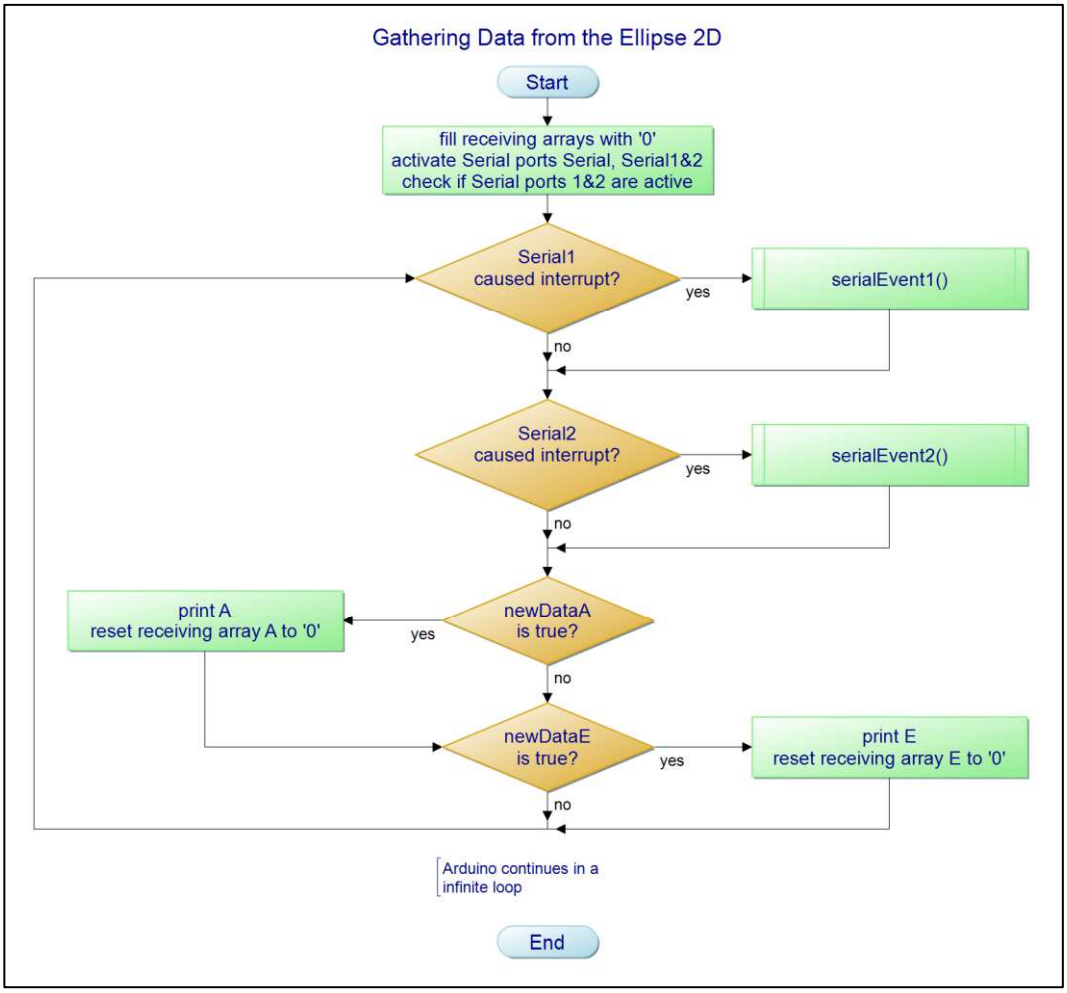

Figure 30: Flowchart that shows the sensor data gathering process.

At the start, the character arrays “RX_A” and “RX_E” that should buffer the received information from the Ellipse2-D, either from port A or port E, need to be defined. Also, the

Boolean variables “newDataA” respectively “newDataE” that indicate if new data has been received, on either serial port 1 or serial port 2, need to be initialised.

In the first part of the program, the setup function, the serial ports have to be set to the correct baud rate (115.200 baud). This should be similar to the Ellipse2-D symbol rate settings (see chapter 3.2.1). To avoid misunderstandings from the microcontroller, arrays should always be initially filled, for example with zeros.

The loop function is an infinite loop in the Arduino programming. It regularly checks if new data has been delivered to either serial port 1 or 2. This process can be interrupted by the serialEvent1() or serialEvent2() interrupt routines (see Figure 31 and Figure 64): Here, they are triggered in case the serial ports register an information flow. The incoming character is saved in a buffer variable and is checked for the start marking character ‘$’. The receiving process starts if ‘$’ could be identified.

The incoming characters are stored in either the “RX_A” or” RX_E” character array until the incoming character is proofed to be the end marking character. This implements to set “newDataA” or “newDataE” as true and the request sees that new data has arrived.

Now, the information buffered in “RX_A” or “RX_E” can be processed further, for example: printed to the serial monitor, stored on the SD-card (see chapter 3.2.3) or transmitted (see chapter 3.3.2).

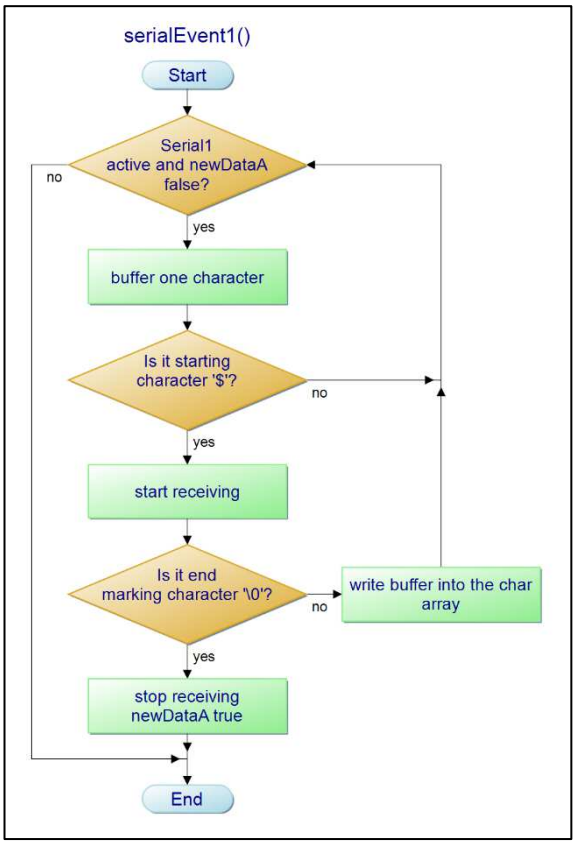

Figure 31: Flowchart of the serialEvent1() interrupt.

3.2.3 Saving the Raw Data on a SD-card

The Ellipse's port E provides the raw data with the NMEA command "PSBGI" with a 5 Hz frequency. These shall be stored on the SD-card as a data backup.

First, the SD-card shield has to be connected to the SPI (serial peripheral interface) on the Arduino board. It is a micro SD-card adapter that is suitable for the Arduino application.

Following pins from the shield also need to be linked (see Table 10):

Table 10: Connection of the SD-card shield to the Arduino Mega 2560.

SD-card Shield	Arduino Mega 2560 SPI
5 V	5 V
Ground	Ground
Data out (DO)	Master in slave out (MISO), pin 50
Data in (DI)	Master out slave in (MOSI), pin 51
Clock (CLK)	Serial clock (SCK), pin 52
Chip select (CS)	Slave select (SS), pin 53

Figure 32 shows an overview of the SD-card code.

First, the SD library has to be included into the program and a file needs to be created. The SD-card needs an active serial port and the chip select pin 53 as an output pin. For the Arduino Mega it is pin 53 (110). After that, the SD-card has to be initialised in the setup routine.

If there is information available that should be stored:

To prevent difficulties in case the last file closing process has failed, the procedure for handling the data with the chosen name is: first close, then reopen it and write the character array. After the print operation is finished the data set has to be closed again.

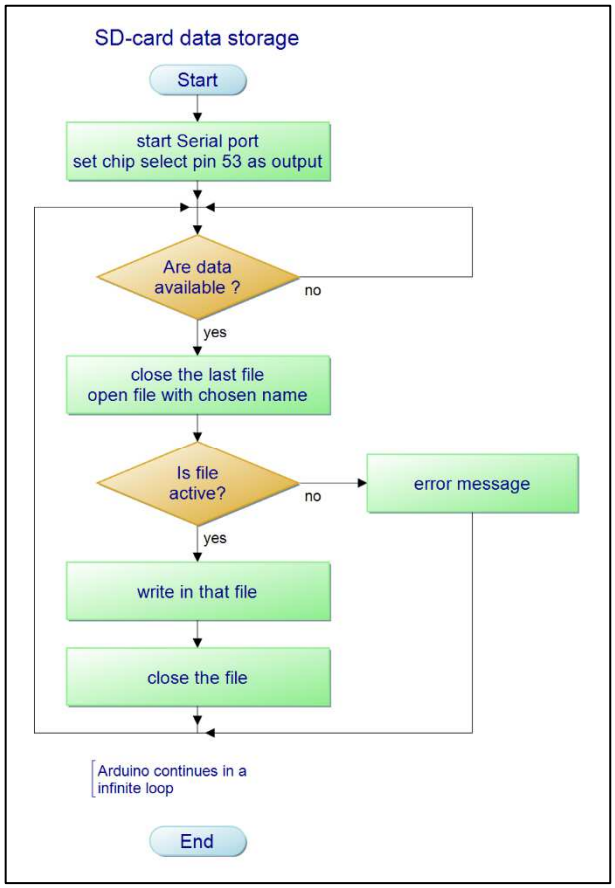

Figure 32: Flowchart of the SD-card code.

3.3 Transmission

3.3.1 First Modem Setup

Both Adeunis 868ULR modems need to be connected with the RS232/USB cable to the computer and the Stand-alone Configuration Manager. There, the baud rate should be set to 115.200 baud and a transmitting channel needs to be chosen (here: channel 11). For the first try, the RF-rate is set on 57,6 kbit/s, this decreases the range but increases the transmission speed. The test if the range is sufficient on site is thematised in a later state of the project.

3.3.2 Transmitting the Data On-shore

Also, for the transmitter a MAX232 level converter is used. Figure 33 shows the schematic drawing in the circuit.

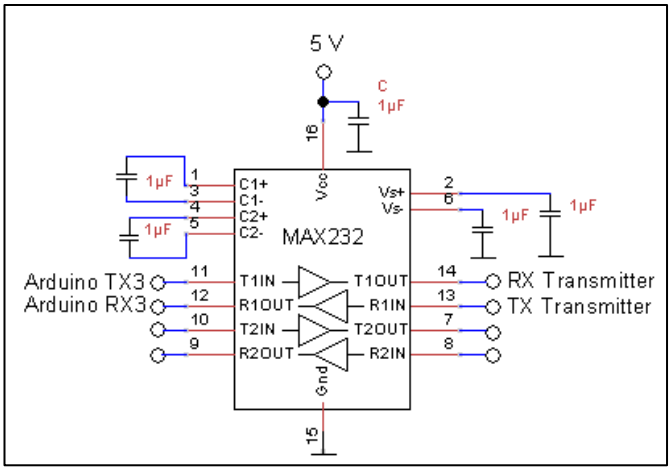

Figure 33: Connection between the transmitter and the Arduino.

The cables from the RS232 connector from the transmitter are linked according to Table 11:

Table 11: Cable connection of the RS232 cable from the transmitter (111).

No.	Colour	Modem RS232 signal	Connection
1	Red	Data carrier detect	To cable 4 and 6
2	Yellow	Received data	To MAX232 Pin 13, R1in
3	Blue	Transmitted data	To MAX232 Pin 14, T1out
4	White	Data terminal ready	To cable 1 and 6
5	Black	Signal ground	To ground
6	Orange	Data set ready	To cable 1 and 4
7	Purple	Request to send	To cable 8
8	Brown	Clear to send	To cable 7
9	Green	Ring indicator	------

Figure 34 shows the flowchart of the data communication part.

Serial port 3 is responsible for the transmitter so it needs to be activated. As soon as there is new data available it broadcasts it automatically.

The first step is to print the via the sprintf() function which formats the data into a string. It has to end with a carriage return (<CR>, '\n') and a line feed (<LF>, '\0') (see chapter 8.3). To send the message, it has to be printed on serial port 3.

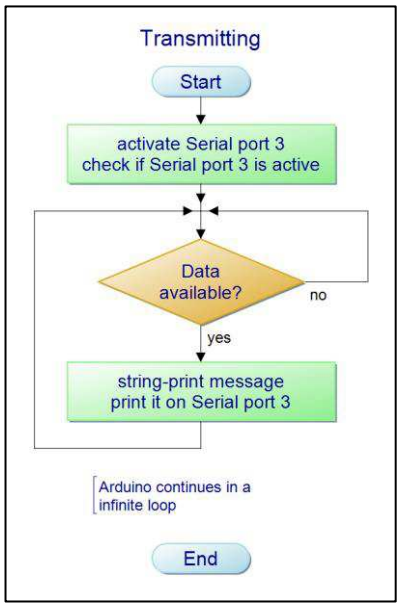

Figure 34: Flowchart transmission part.

3.4 Summary of the Code

The whole programming code can be found in chapter 8.3. Here, already explained parts of the code are placed in one flow. (see Figure 35)

As the serial port and serial port 1, 2 and 3 (see Table 12) are using 115.200 baud, they all must be enabled accordingly. Also, all setup routines from the measurement system and the SD-card code need to be included.

Table 12: Serial ports usage.

Serial port	SD-card
Serial port 1	Ellipse2-D port A
Serial port 2	Ellipse2-D port E
Serial port 3	Adeunis Transmitter

The program waits for interrupts from serial port 1 and serial port 2. If it registers a data income from for example serial port 1, which includes the calculated values from the sensor in the "PASHR" command, they are sent through the radio transmission system.

As soon as serial port 2 picks up new data, the indicator variable “newDataE” sets to status “true”. Afterwards, this data which includes the transmitted raw data from the Ellipse2-D is stored on the SD-card.

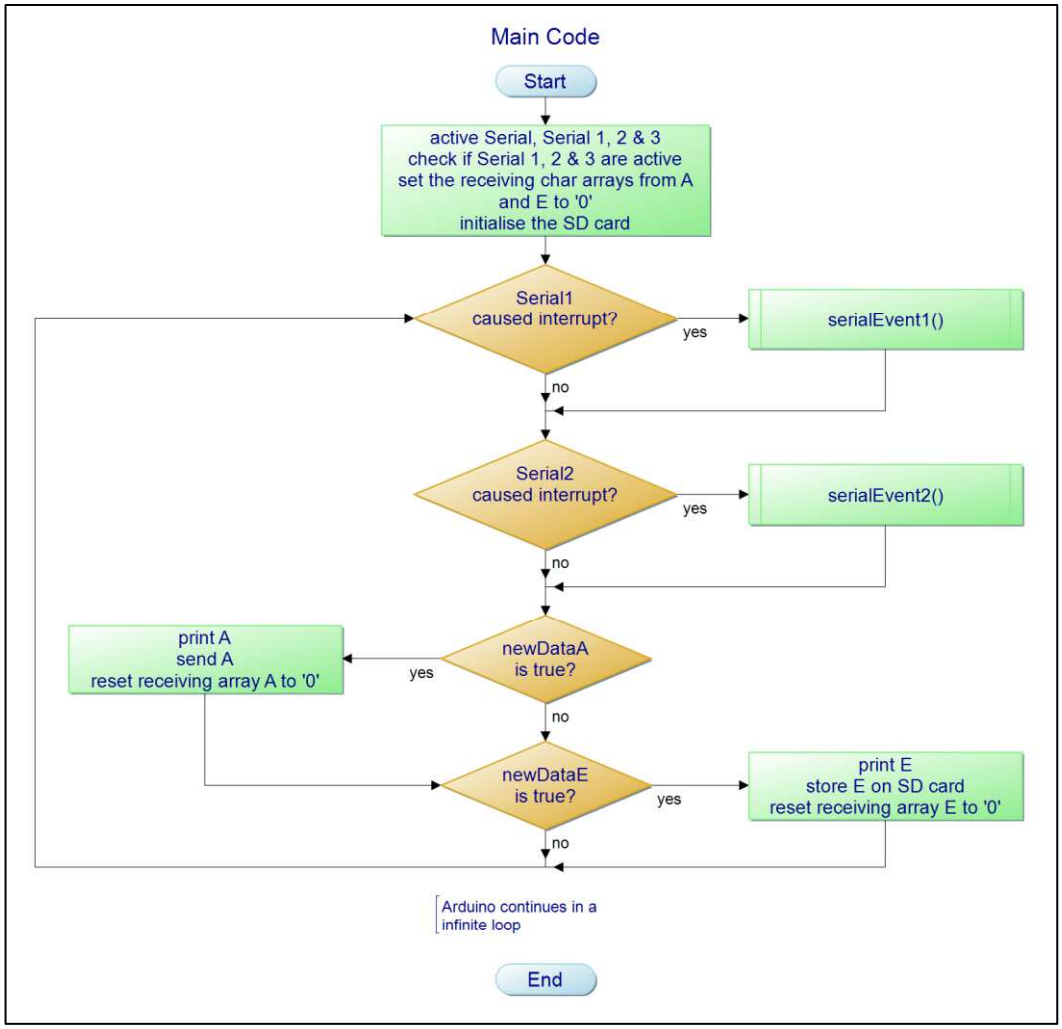

Figure 35: Flowchart of the whole code.

4 Results and Discussion

This part summarises the outcome from chapter 2 and 3. It explains which components are finally chosen (for an overview see chapter 8.1.1 and 8.1.2) and the testing phase of the project.

4.1 Power Supply

Note: As the buoy will not be delivered (incl. the end application battery and solar panel), there is a smaller battery and solar panel ordered for the testing process in the summer 2020.

For the testing sessions during summer 2020, a lighter and smaller battery with 30 Ah is chosen: Varta 53030 (see chapter 2.4.1). This will be replaced by a 60 Ah battery in the end application to increase the energy security to buffer times with less sunlight.

The solar panel for the testing in summer 2020 according to chapter 2.4.2 should have a higher peak power than 16 W_{peak}. Therefore, one saltwater-proof SunWare 20163 solar panel with 25 W_{peak} is chosen.

Because the end application is also used in winter, the solar panel should not be scaled beyond 55 W_{peak}: The decision is made for four panels that will be attached to the steel structure on top of the buoy. The ordered solar panels will provide 15 W_{peak} each. As the buoy will not face a static cardinal direction it will be better to assemble those facing in different directions. With this, a power of maximal 60 W_{peak} can be reached.

Another advantage of several panels is that there are more possibilities in changing the voltage or the current due to the opportunity of parallel or serial connection.

Furthermore, one 60 W_{peak} solar panel is heavy and large sized. This will have an influence of the initial position of the buoy in the water due to unbalance or its higher wind sensitivity.

4.1.1 Testing

A 48 hours test is planned with the SunWare 20163 solar panel and the 30 Ah-Varta 53030: The running system is placed next to a window inside the university building of Uppsala university. The test is started with a battery voltage of 12,02 V. After 48 hours the battery voltage measures only 11,7 V and the system shut down through the charge controller to protect the battery from deep-discharge. The weather was half a day cloudy and the rest of the time sunny. Also, the short Swedish summer nights support a high income of light on the panel.

One explanation is that the irradiation that enters the solar panel through the window is probably very low.

A second test is made for several hours and it could be seen that the battery voltage immediately recovers and increases. This time the solar panel was placed outside.

In the end it can be ascertained that in a time frame of 24 hours (from morning to the next morning), the battery voltage increases from 11,7 V to 12,23 V and the system restarts already shortly after being exposed to the sun. The 24 hours were fsunny and also here, the Swedish summer nights helped that a lot of light can reach the panel.

4.2 Measurement

The sensor unit is connected to the Arduino and information from both ports can be received and read out on the coupled communication port (COM port) or can be saved on the SD-card.

To evaluate the sensor unit, three different tests are made:

- Static testing
- Dynamic testing of the gyroscope with a robot
- Dynamic testing of the accelerometer in an elevator

4.2.1 Static Test

In the static test, the Ellipse2-D is kept without motion on a table in the laboratory. Before the test starts, it is connected for about one hour before so that the electronics could warm up and the result is not influenced by a temperature shift.

Figure 36 to Figure 41 show the raw data that are sent on port E with the NMEA command "PSBGI":

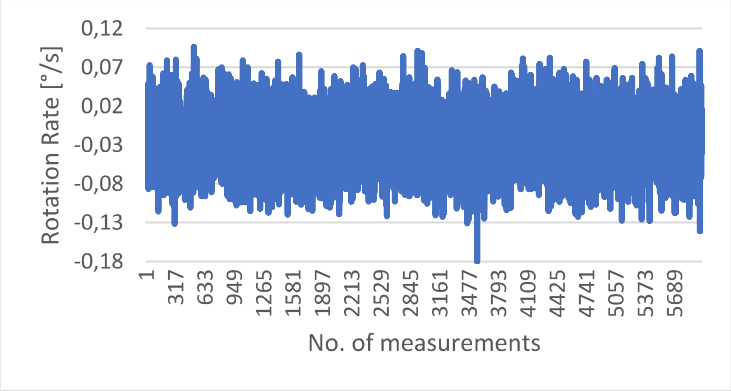

Figure 36: Static test gyroscope X-axis.

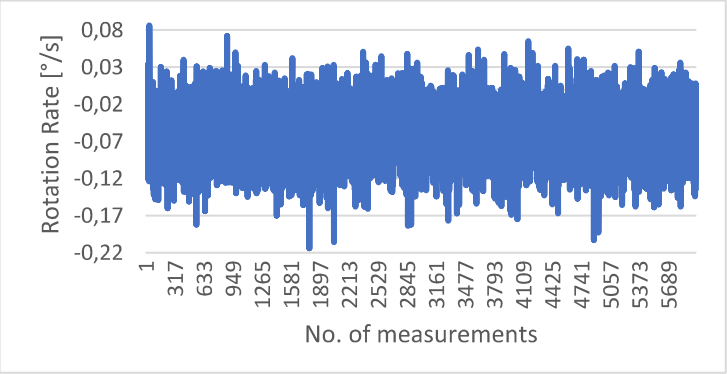

Figure 37: Static test gyroscope Y-axis.

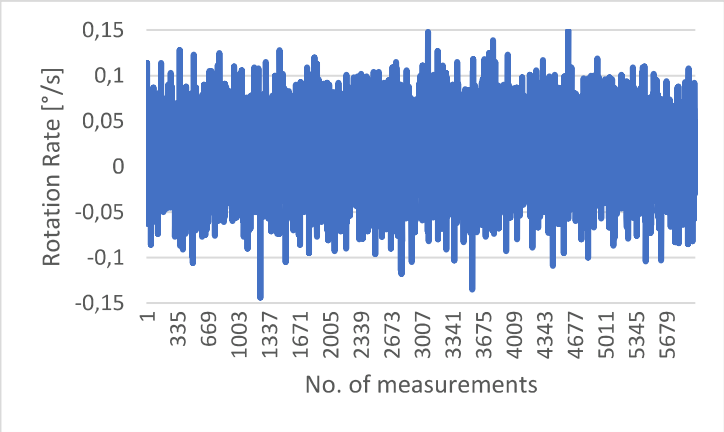

Figure 38: Static test gyroscope Z-axis.

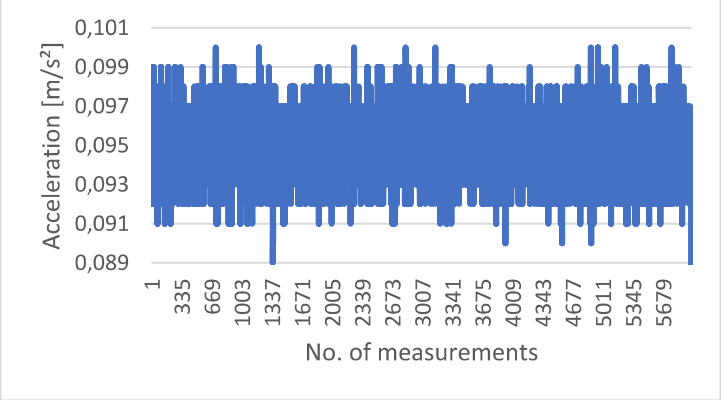

Figure 39: Static test accelerometer X-axis.

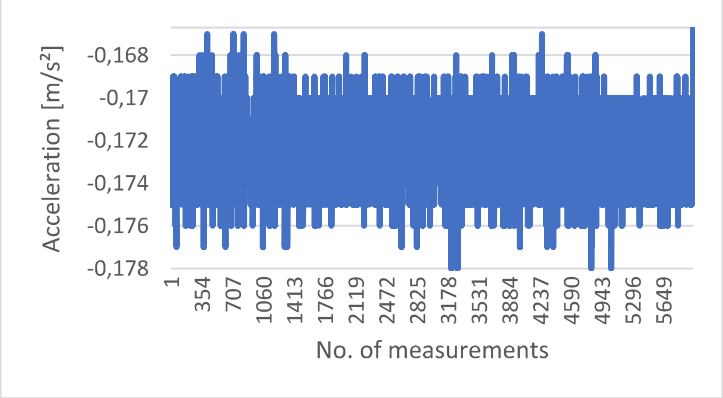

Figure 40: Static test accelerometer Y-axis.

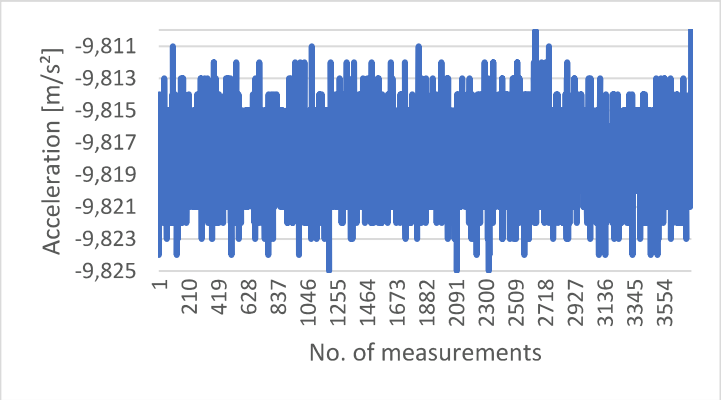

Figure 41: Static test accelerometer Z-axis.

Table 13 shows an overview of the measurement results that are presented above. It is expected that the measured rotation rates are approximately zero, as in a static state no rotation occurs. This is also predicted for the accelerometers that are not influenced by the gravitational force of the Earth. As the sensor unit is placed in its initial position, the gravity acts on the Z-axis. The gravitational force in Sweden is around 9,82 m/s² and as the Z-axis is orientated against the force, it is displayed negative.

Table 13: Static test for the gyroscopes (Gyro) and the accelerometers (Acc).

	Rotation rates [°/s]			Acceleration [m/s²]		
	Gyro X	Gyro Y	Gyro Z	Acc X	Acc Y	Acc Z
Min.	-0,180	-0,214	-0,144	0,089	-0,178	-9,825
Max.	0,096	0,086	0,150	0,100	-0,167	-9,810
Average	-0,024	-0,060	0,014	0,095	-0,1724	-9,818
Standard deviation	0,036	0,036	0,037	0,0015	0,0015	0,002

Two points can be seen clearly:

- The sensor outputs differ in some points but do not drift away, that means that the sensor does for example not metaphorically speaking “start to move up- or downwards or to turn” referring to the data. The differences can be explained from noises that are everywhere in the surroundings.
- The standard deviations are low. This shows that the measured data is not widely spread around the average value.

4.2.2 Dynamic Test

Gyroscope:

For the dynamic test of the gyroscope, the robot in the division of electricity at Uppsala University is used. It can be programmed to exact one 360° turn and the settings can be adjusted easily. The test is made for all the three spatial axes: In alternation the robot arm is turned ten times clockwise and anticlockwise. Following conditions are noted (see Table 14):

Table 14: Testing conditions dynamic tests gyroscope.

Rotation:	360 °
Measured radius of the robot head:	r = 14 cm
Calculated Perimeter:	$U = 2\pi r = 88\ cm$
Measured time for one full turn:	t = 11,1 s
Frequency data input from Ellipse2-D	f = 5 Hz
Calculated data input cycle time from f	$t_{meas} = \frac{1}{5\ Hz} = 0{,}2\ s$

With this, following assumption can be made:

The robot arm turns 360° in approximately 11,1 s, which leads to 0,03 s per degree.

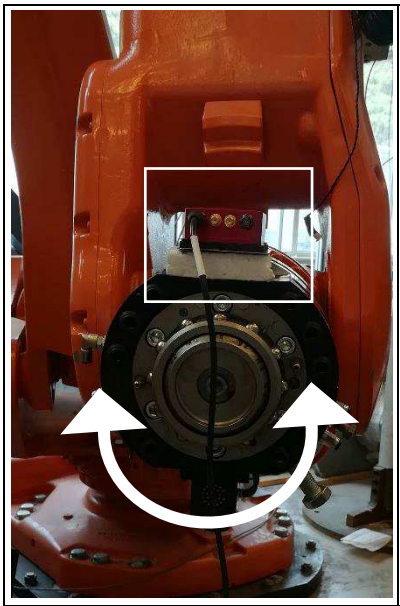

Figure 42: Dynamic test gyroscope X-axis.

Figure 43: Dynamic test gyroscope Y-axis.

Figure 44: Dynamic test gyroscope Z-axis.

Figure 42 to Figure 44 show the testing setup for the respective axis, whereas Figure 45 illustrates the orientation of the Ellipse2-D.

Figure 45: Orientation of the Ellipse2-D.

In Figure 42 to Figure 45 it can be observed that the Ellipse2-D is not placed in the centre of rotation. To compensate this through the software that is included in the system, following offset settings are given to the sensor unit (see Table 15):

Table 15: Offset settings for the gyroscope dynamic test.

	Roll	**Pitch**	**Yaw**
X	Can be neglected	+ 0,11 m	+ 0,17 m
Y	0 m	Can be neglected	0 m
Z	+ 0,14 m	+ 0,14 m	Can be neglected

Testing of the Gyroscope of the X-axis (Roll Angle):

Figure 46 and Figure 47 display the calculated decimal angles in degree for the clockwise and anticlockwise motion. Both figures show that all 10 series of measurements for the anticlockwise and the clockwise tests show the same behaviour. It is clear that the repetitions are similar.

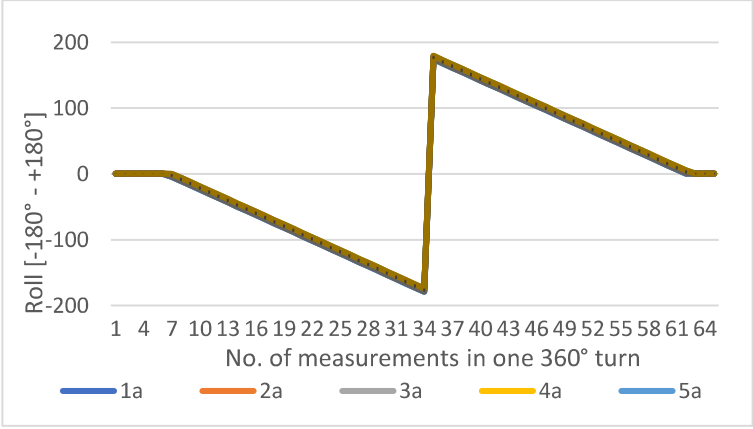

Figure 46: Roll [°] anticlockwise.

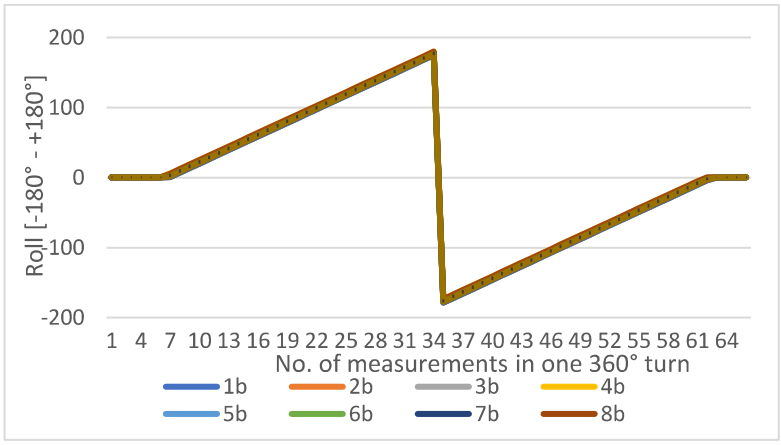

Figure 47: Roll [°] clockwise.

Figure 48 demonstrates the rotation rate in degree per second for the anticlockwise – Figure 49 shows the same data for the clockwise setting.

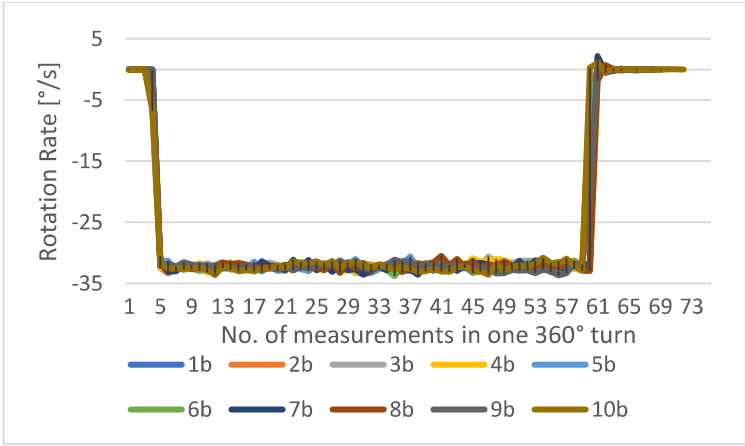

Figure 48: Rotation rate from gyroscope X-axis [°/s] anticlockwise.

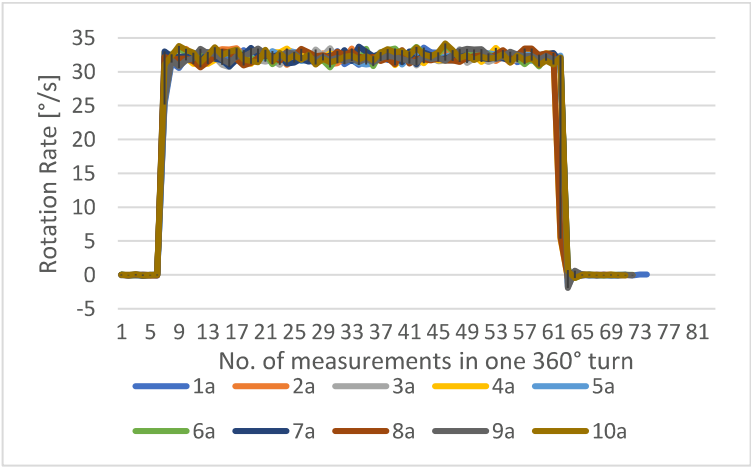

Figure 49: Rotation rate from gyroscope X-axis [°/s] clockwise.

Table 16 helps to prove the assumption that is stated at the beginning of this chapter. The calculations include the parameters that are measured at the start of the experiment and are written down in Table 14.

Table 16: Calculation of the time per degree for the gyroscope X-axis both directions.

	Anticlockwise	**Clockwise**
Measurement set No.	1a	1b
No. of taken measurements during 360° turn	55	56
Total time for the 360° turn [s]	$55 * 0{,}2\ s = 11$	$56 * 0{,}2\ s = 11{,}2$
Average rotation rate [°/s]	32,05	32,09
Time per degree	0,031	0,031

These calculations state that the times per degree are similar to the assumptions.

Testing of the Gyroscope of the Y-axis (Pitch Angle):

In Figure 50 and Figure 51 the calculated decimal angles in degree from the Kalman model; both, clock- and anticlockwise are demonstrated:

All 10 series of measurement for the clockwise test show the same pattern which implies that the repetitions are similar. Whereas No. 7a in the anticlockwise row behaves a little bit delayed compared to the remaining 9. It still shows clear similarities.

If this problem occurs due to a sensor error or a robot issue it cannot be explained.

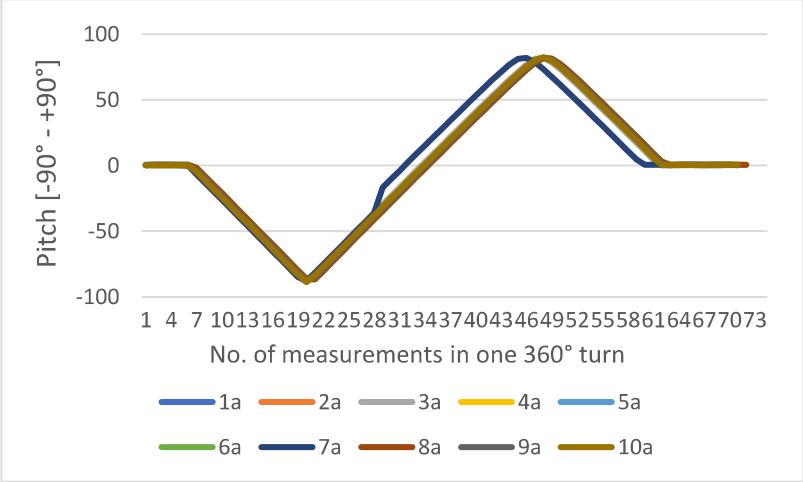

Figure 50: Pitch [°] anticlockwise.

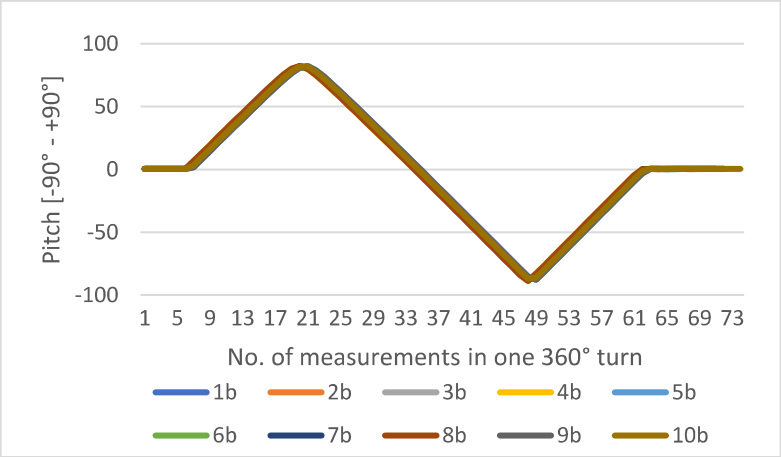

Figure 51: Pitch [°] clockwise.

The rotation rates in degree per second can be seen in Figure 52 (anticlockwise) and Figure 53 (clockwise).

The Figure 52 (anticlockwise) has some sparks in the first two series. Here, the cable could not follow the robot movement smoothly. To remedy this, a part of the cable is fixed to the robot. This improves the results for the following eight series.

In addition to this, in both data presentations, there are noises at the start and the end of every measurement series: Because the fixation of the Ellipse2-D to the robot is difficult, a metal plate is used. This causes vibrations when speeding up and slowing down the robot, noticeable as noisy interference.

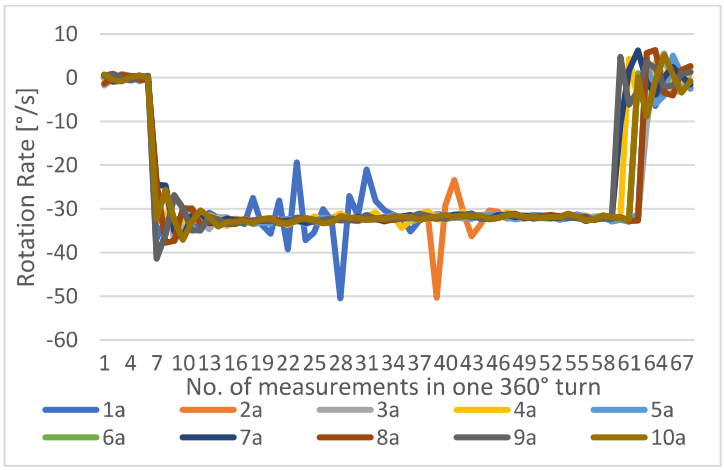

Figure 52: Rotation rate from gyroscope Y-axis [°/s] anticlockwise.

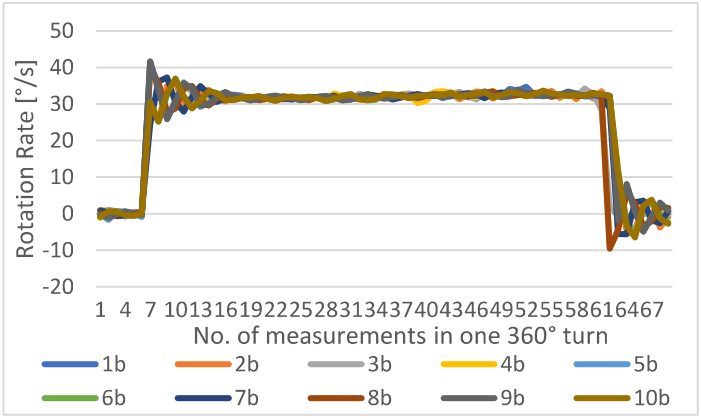

Figure 53: Rotation rate from gyroscope Y-axis [°/s] clockwise.

Table 17 displays the way of calculation that is needed to compare the measurement results with the assumption above.

Table 17: Calculation of the time per degree for the gyroscope Y-axis both directions.

	Anticlockwise	**Clockwise**
Measurement set No.	4a	7b
No. of taken measurements during 360° turn	54	56
Total time for the 360° turn [s]	$54 * 0{,}2\ s = 10{,}8$	$56 * 0{,}2\ s = 11{,}2$
Average rotation rate [°/s]	32,11	32,01
Time per degree	0,031	0,031

It is shown that the measurements match with the assumption.

Testing of the Gyroscope of the Z-axis (Yaw Angle):

Note: The sensor itself measures gyroscope rotation rates on all three axes. Whereas the Kalman model provides just values for the pitch and roll motions.

Figure 54 and Figure 55 display the rotation rate for the anticlockwise and the clockwise experiments. Similar to the Y-axis measurements, the fixture is also with low stiffness why vibrations and noises can be seen in both figures.

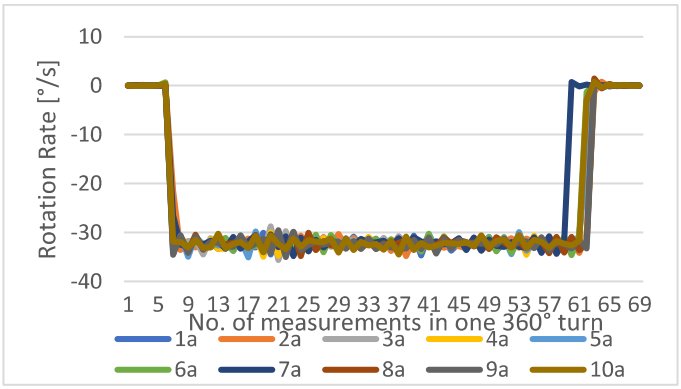

Figure 54: Rotation rate from gyroscope Z-axis [°/s] anticlockwise.

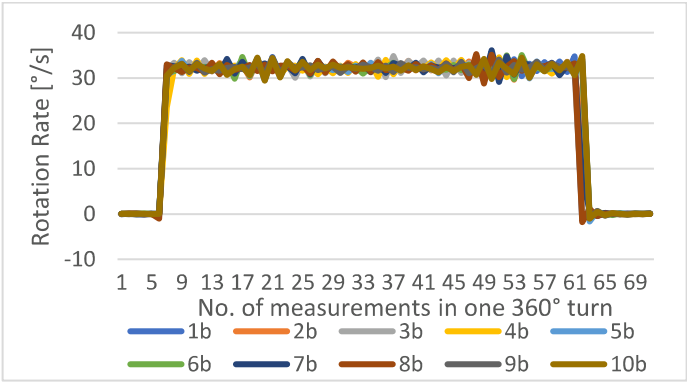

Figure 55: Rotation rate from gyroscope Z-axis [°/s] clockwise.

In Table 18 the time per degree is determined:

Table 18: Calculation of the time per degree for the gyroscope Z-axis both directions.

	Anticlockwise	**Clockwise**
Measurement set No.	5a	8b
No. of taken measurements during 360° turn	56	55
Total time for the 360° turn [s]	$54 * 0{,}2\ s = 11{,}2$	$55 * 0{,}2\ s = 11$
Average rotation rate [°/s]	32,03	32,31
Time per degree	0,031	0,031

Also, the Z-axis satisfies the expectations from the beginning.

Accelerometer:

Note: Due to the point that there is no GNSS reception inside the elevator, the Kalman model was excluded in this part of the sensor evaluation.

The accelerometer is tested in an elevator to simulate a controlled motion in one direction. Every axis measures 10 times a ride upwards as well as downwards. The motions that occur between the movements, for example due to doors or walking are cut out for a great extent.

The elevator drives always five floors: from the K1 to the 4th floor and back. K1 describes the level under the ground floor. One ride takes ca. 35 seconds and one floor is estimated 4 m high.

After one measurement series (10 times up and down), the sensor has to be turned so that the acceleration of the ride acts on another axis.

Figure 56 displays the process of an upwards ride; Figure 57 illustrates a downwards ride.

Both can be split into three parts:

- Starting up
- The ride itself
- Braking

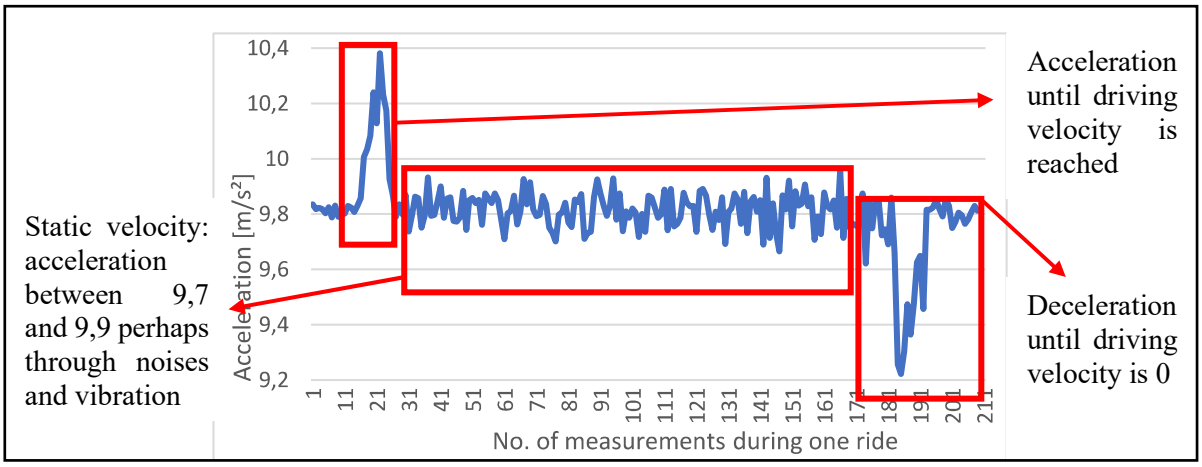

Figure 56: 6th upwards ride acceleration "X-axis" [m/s²].

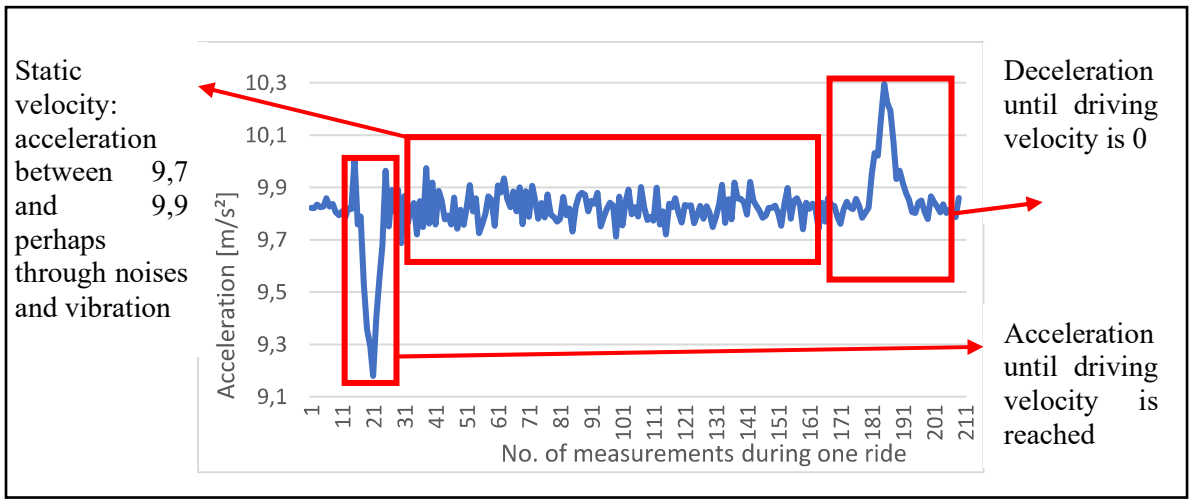

Figure 57: 2nd downwards ride acceleration "X-axis" [m/s²].

On the basis of Figure 58 to Figure 60 which show the acceleration in m/s² for each of the three axes for driving upwards it can be said that the foundation of the curves is similar. Sometimes, the peak looks shifted (see Figure 60 the braking peak of the elevator), the slope differs (see Figure 59, the acceleration peak of the elevator ride) or the height of the peak varies (see Figure 59, the braking peak of the elevator).

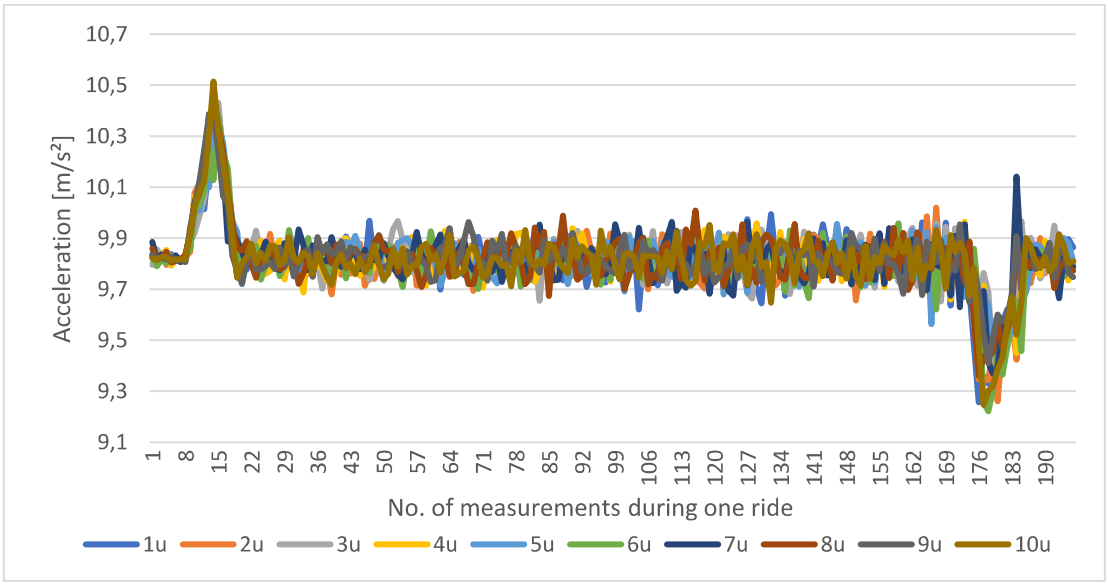

Figure 58: Acceleration for the accelerometer X-axis [m/s²] for upwards.

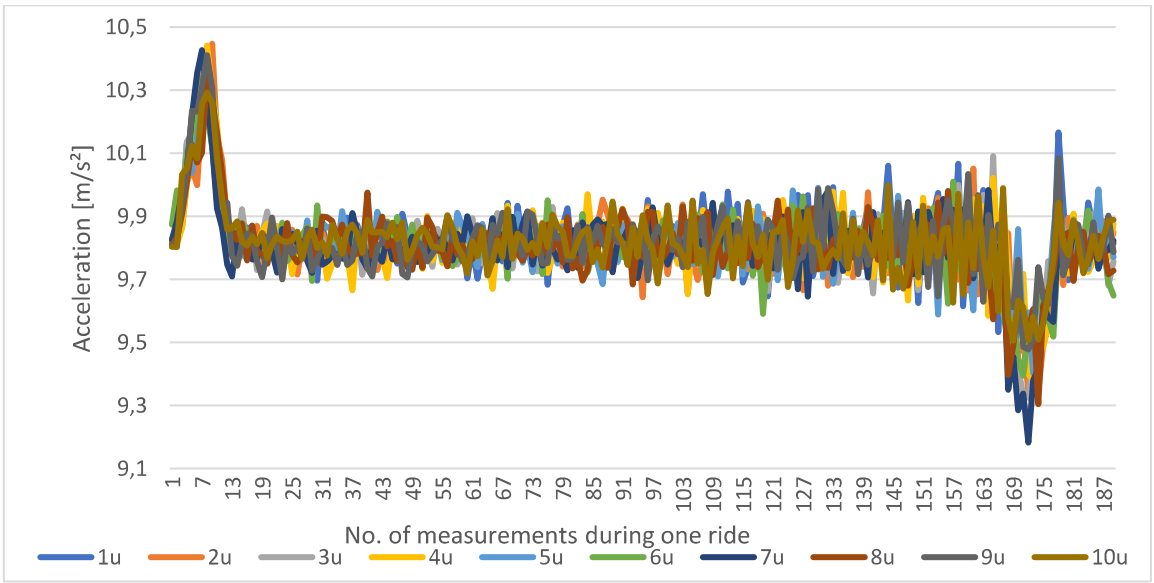

Figure 59: Acceleration for the accelerometer Y-axis [m/s²] for upwards.

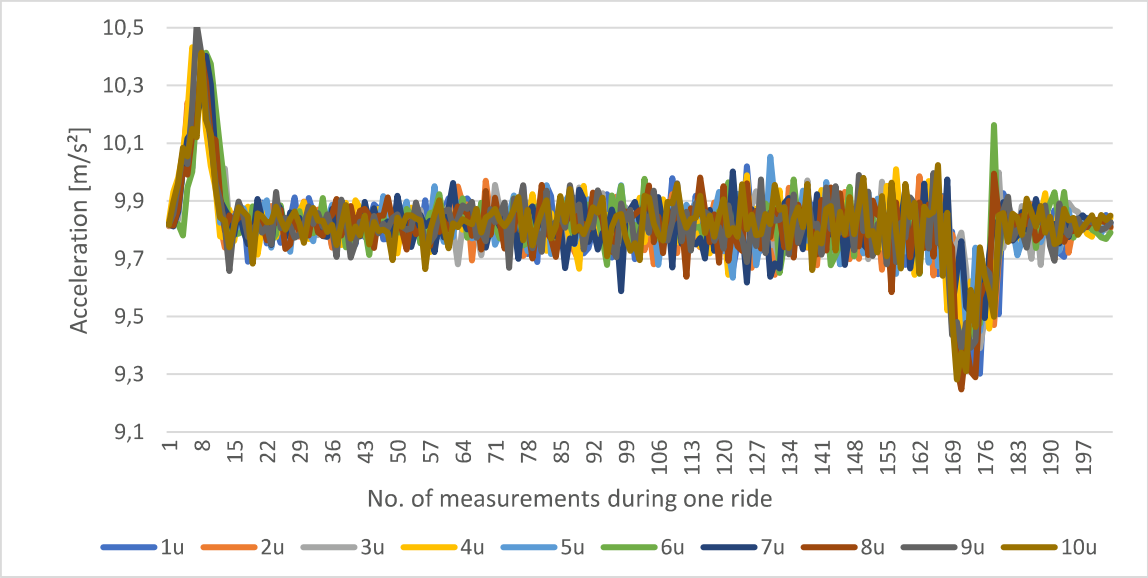

Figure 60: Acceleration for the accelerometer Z-axis [m/s²] for upwards.

For the accelerometer measurements from the downwards motion (see Figure 61 to Figure 63) characteristics can be observed:

- Slope (see Figure 62, at the starting process)
- Peak shifting (see Figure 63, at the braking process)
- Height of peak differences (see Figure 61, at the starting process).

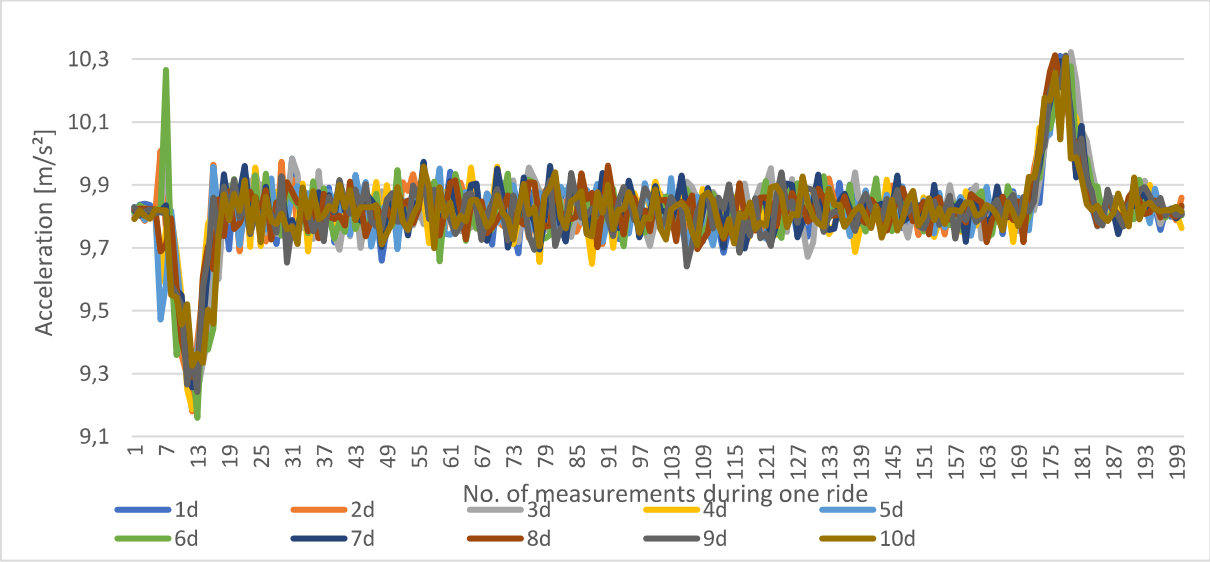

Figure 61: Acceleration for the accelerometer X-axis [m/s²] for downwards.

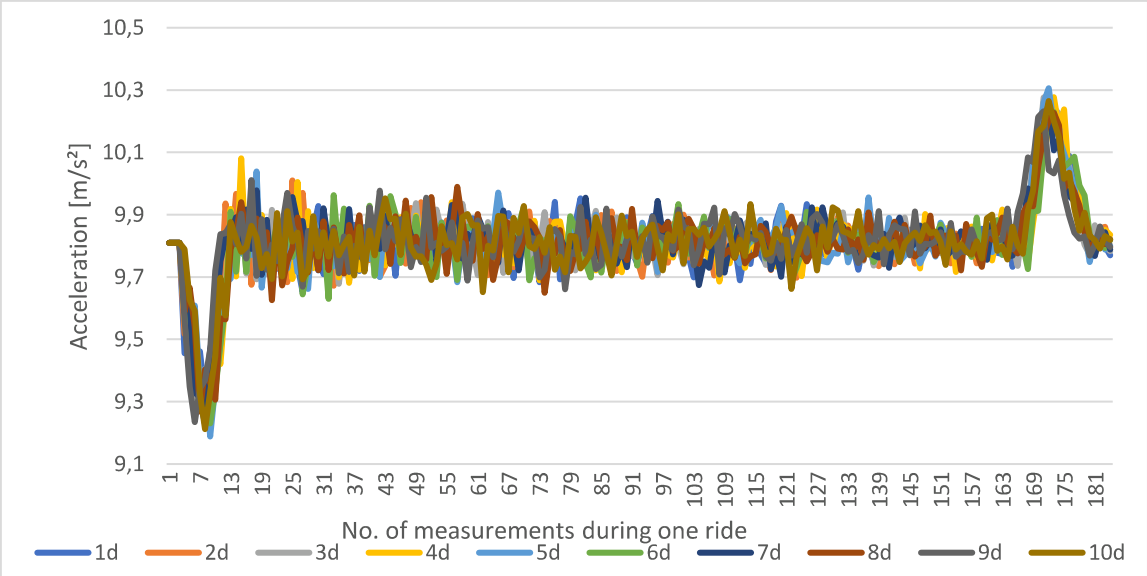

Figure 62: Acceleration for the accelerometer Y-axis [m/s²] for downwards.

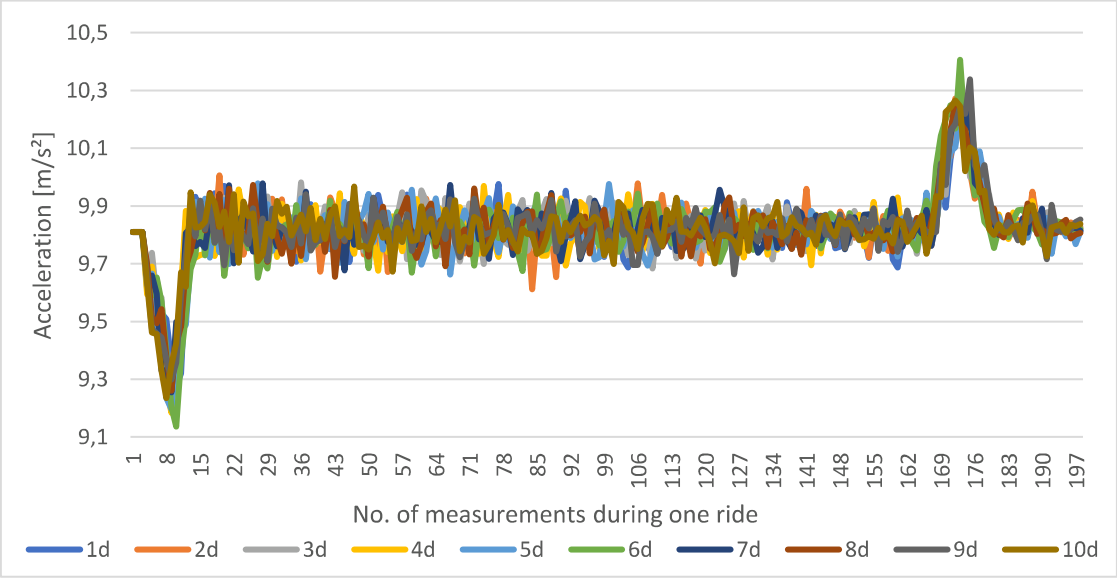

Figure 63: Acceleration for the accelerometer Z-axis[m/s²] for downwards.

Overall, it can be stated that the behaviour of the accelerometer appears to be similar.

The differences in the characteristics have varied origins, for example vibrations or the elevator machinery itself. In addition to that, the sensor is not fixed to a proper and stable structure which supports further appearance of vibrations.

It is clear to see that there is a defined motion that occurs with every measurement series.

4.3 Data Transmission

To test the transmission system, a distance test is made. Here, the range of the transmission system is tested above a fresh water surface and on the countryside. Challenges that have been encountered during these tests:

- Measurement on the lake: houses and trees, weather and seasons also have an influence on the transmission
- Measurement on the countryside: landscapes are seldom totally flat, trees, transmission lines and houses have an impact on the communication

For the countryside experiment, a rural area around Uppsala is found:

Start point: 59°48’17.2’’N, 17°45’54.4’’E

End point: 59°47’13.0’’N, 17°48’35.8’’E

Reached range: 3,2 km

For the lake experiment, it has been cycled around the lake in Hagaparken, Solna:

Start point: 59°22’45.2’’N, 18°01’13.3’’E

End point: 59°21’13.5’’N, 18°02’34.3’’E

Reached range: 3,3 km

The system should be able to achieve a range of 20 km under good conditions (low noise and reflection impacts). (90) Due to the increased transmission speed, the range is stated to halve. (112)

In the end, a range of about 3 km can be reached, that is, regarding to the circumstances (site characteristics) acceptable. For the further project progress, it should be decided if a better transmission system is needed. To verify this, a test above salt water is mandatory.

5 Conclusion

A measurement system that quantified acceleration and rotation in all three spatial axes was designed and the task of the project was realised:

The Arduino Mega 2560 was connected to the Ellipse2-D AHRS/INS and was able to pick up the data, and the radio transmission system was capable of sending data about a 3 km range in not ideal conditions.

A detailed description of the programming code and the design of the circuit had been presented. In addition to that, the mandatory software settings had to be adjusted for the listed components.

The graphs of the evaluation of the sensor unit's accelerometer and gyroscope were showcased and interpreted. As expected, the results of the measurement series were coherent and reasonable. Also, they could be replicated under the same conditions.

In the next steps of the project, the circuit will be implemented in the buoy and tested under real conditions on-site.

6 Future Work

This paragraph explains the next possible steps of the project. During the project work some things pointed out that could be useful to implement or have to be included to be able to use the buoy in the end.

The **circuit setup** from the breadboard should be soldered on a Printed Circuit Board (PCB) to avoid loose cables or short circuits during the operational phase and to achieve a stable setting.

After the delivery of the **buoy**, the components have to be fixed safely into the battery- and the electronic-boxes that have been ordered with the buoy. Even though, an extra pole needs to be welded on top of the steel structure for the GNSS antennas.

The solar panels and the battery that will be delivered with the buoy have to be connected and tested. Afterwards, the circuit is required to be linked to the **power supply**.

The solar panels that will be delivered later provide a voltage of 18 V and a short circuit current of 21,8 A per panel according to the quotation of the buoy company. There will be in total four panels assembled. The LS1024EU charge controller that was used in the first test build-up can handle a maximum current of 10 A. Therefore, a higher rated charge controller has to be implemented into the system.

If the system rate or range on-site is not sufficient, the **transmission system** needs to be replaced as it supports a maximal baud rate of 115.200 baud (see chapter 6).

The **GNSS antennas** should be installed with a minimal distance of 50 cm to each other on the buoy structure. The connectors have to face the same direction and are required to be sealed with amalgamating tape.

In the software sbgCenter Application, the settings according to the distance between the Ellipse2-D and the antennas have to be implemented to increase the AHRS/INS accuracy.

It needs to be checked if **the system rate** is sufficient. If required, it is necessary to increase the baud rate. Therefore, another level converter, a communication system and possibly another microcontroller must be implemented as the actual parts are restricted to 115.200 baud.

To avoid a hang-up of the **programming** as the Arduino is in an infinite loop a watch dog function should be implemented to reset the microcontroller if necessary.

Furthermore, it is also essential to evaluate a method to **calibrate the magnetometer**. Therefore, the device has to be guided through specific movements. This should be conducted preferably in the final setup and in a surrounding with less interferences. Challenging hereby is the weight of the buoy (~100 kg) without any additional components.

The **receiver** of the transmission system has to be installed in the office in Kristineberg. It is planned to connect the receiver via a RS232 interface to a Raspberry Pi which transmits the received sensor data via Wi-Fi to a computer and through a **server** from Kristineberg to Uppsala.

In addition to this, a server system has to be found that is able to transport the information further to Uppsala. At the moment there is already contact to Moxa Inc., as there is already a system running for a similar purpose.

After assembling all the components into the buoy, it needs to be **tested** on-site in Lysekil, Sweden. Therefore, the range of the radio communication system has to be verified under real environmental conditions (salt water, heavy rain, high waves).

7 References

1. Bernhoff H. [edits.]. Wave power compendium: Technology, environment and system [Compendium]. Uppsala University, Sweden.

2. Send U, Regier L, Jones B. Use of Underwater Gliders for Acoustic Data Retrieval from Subsurface Oceanographic Instrumentation and Bidirectional Communication in the Deep Ocean. Journal of Atmospheric and Oceanic Technology 2012; 30(5):984–98.

3. Wyatt LR, Thompson SP, Burton RR. Evaluation of high frequency radar wave measurement. Coastal Engineering 1999; 37(3-4):259–82.

4. The European Marine Energy Centre Limited. Wave devices [accessed 2020 Jun 23]. Available from: URL: http://www.emec.org.uk/marine-energy/wave-devices/.

5. Falcão AFO, Henriques JCC. Oscillating-water-column wave energy converters and air turbines: A review. Renewable Energy 2016; 85:1391–424.

6. Kofoed JP. Wave overtopping of marine structures [Doctoral dissertation, Ph. D. thesis]. Denmark: Aalborg University; 2002.

7. Bull D, Ochs ME. Technological Cost-Reduction Pathways for Attenuator Wave Energy Converters in the Marine Hydrokinetic Environment [Tech. Rep.]; 2013.

8. Holmberg P, Andersson M, Bolund B, Strandanger K. Wave Power - Surveillance study of the development: Elforsk rapport 11:02 May 2011.

9. Whittaker T, Folley M. Nearshore oscillating wave surge converters and the development of Oyster. Philos Trans A Math Phys Eng Sci 2012; 370(1959):345–64.

10. Folley M, Whittaker T, Osterried M. The Oscillating Wave Surge Converter. Proceedings of the International Offshore and Polar Engineering Conference 2004.

11. The European Marine Energy Centre Limited. Aquamarine Power [accessed 2020 Jun 24]. Available from: URL: http://www.emec.org.uk/about-us/wave-clients/aquamarine-power/.

12. Farrok O, Ahmed K, Tahlil AD, Farah MM, Kiran MR, Islam MR. Electrical Power Generation from the Oceanic Wave for Sustainable Advancement in Renewable Energy Technologies. Sustainability 2020; 12(6):2178.

13. Wello Oy. Penguin’s competitive advantage [accessed 2020 Jun 24]. Available from: URL: https://wello.eu/technology/.

14. Chatzigiannakou MA, Ulvgård L, Temiz I, Leijon M. Offshore deployments of wave energy converters by Uppsala University, Sweden. Mar Syst Ocean Technol 2019; 14(2-3):67–74.

15. Seabased Group. The Technology [accessed 2020 Jun 17]. Available from: URL: https://www.seabased.com/the-technology.

16. Richter M, Magana ME, Sawodny O, Brekken TKA. Nonlinear Model Predictive Control of a Point Absorber Wave Energy Converter. IEEE Trans. Sustain. Energy 2013; 4(1):118–26.

17. Castellucci V, Abrahamsson J, Kamf T, Waters R. Nearshore Tests of the Tidal Compensation System for Point-Absorbing Wave Energy Converters. Energies 2015; 8(4):3272–91.

18. Krell M, Jonsson L. Evaluating the Potential of Seabased's Wave Power Technology in New Zealand [Master Thesis]. Uppsala University, Sweden; 2011.

19. Parwal A. Grid Integration and Impact of a Wave Power System [Doctoral thesis]. Uppsala University, Sweden; 2019.

20. Blavette A, O'Sullivan D, Egan MG, Lewis T. Grid compliance of ocean energy converters: Control strategies and recommendations 2011.

21. Tyrberg S, Svensson O, Kurupath V, Engstrom J, Stromstedt E, Leijon M. Wave Buoy and Translator Motions—On-Site Measurements and Simulations. IEEE J. Oceanic Eng. 2011; 36(3):377–85.

22. Waters R, Engström J, Isberg J, Leijon M. Wave climate off the Swedish west coast. Renewable Energy 2009; 34(6):1600–6.

23. Waters R. Lysekilsprojektet: Uppsala University, Sweden [accessed 2020 Jun 6]. Available from: URL: https://www.teknik.uu.se/elektricitetslara/forskningsomraden/vagkraft/lysekil/.

24. Bochert A, Boelmann J, Temiz I. [edits.]. Proceedings of the Sixth Workshop for Maritime Technologies at the Sven Lovén Centre: July 1 to July 5, 2019. Hochschule Bremerhaven, Uppsala Universitet; 2019.

25. Lüer J, Ullah MI, Ringe S. Thematic Studies in Renewable Electricity Production, 1TE677: Project: Generate Wave Data [Project Report]. Uppsala: Uppsala University, Sweden; 2019.

26. Stetenfeldt A. Data communication for near shore applications [Master Thesis]. Uppsala University, Sweden; 2017.

27. Sandurawan D, Kodikara N, Keppitiyagama C, Rosa R. A Six Degrees of Freedom Ship Simulation System for Maritime Education. Int J on Adv. in ICT for Emerging Countries 2011; 3(2):34.

28. Hesse S, Schnell G. Sensoren für die Prozess- und Fabrikautomation: Funktion - Ausführung - Anwendung. 6., korr. und verb. Aufl. Wiesbaden: Springer Vieweg; 2014.

29. Balluff GmbH. Funktion, Aufbau und Technologien von Sensoren: Wie Sensorik funktioniert [accessed 2020 Jan 24]. Available from: URL: https://www.balluff.com/local/ch/service/basics-of-automation/fundamentals-of-automation/basic-of-sensing/.

30. Balluff GmbH. Technisches Glossar: "U" [accessed 2020 Jan 24]. Available from: URL: https://www.balluff.com/local/ch/glossary/technical-glossary/.

31. NIHON DEMPA KOGYO CO. Ultrasound and its properties; 2018 [accessed 2020 Jun 2]. Available from: URL: https://www.ndk.com/en/sensor/ultrasonic/basic01.html.

32. Shao L, Xie G. Real-time tracking of moving objects on a water surface. In: International Conference on Mechatronics and Automation (ICMA), 2012: 5 - 8 Aug. 2012, Chengdu, China. Piscataway, NJ: IEEE; 2012. p. 2114–9.

33. Fraunhofer-Institut für Siliziumtechnologie. Drehratensensoren / Inertialsensoren; 2018 [accessed 2020 Feb 11]. Available from: URL: https://www.isit.fraunhofer.de/de/mikro-fertigungsverfahren/prozessintegration-und-pilotfertigung1/polysilizium-technologieplattform/drehratensensoren-inertialsensoren.html.

34. Breuer J, Kutschker A. Funktionsweise einer IMU (Inertial Measurement Unit): Großes Projekt: Sondierung mit unbemannten Luftfahrtsystemen [Course Material WS 15]: Universität Augsburg; 2015.

35. STMicroelectronics. MEMS Gyroscopes [accessed 2020 Apr 8]. Available from: URL: https://www.youtube.com/watch?v=l75IiNVRdfg.

36. VectorNav Technologies. Inertial Measurement Units and Inertial Navigation; 2020 [accessed 2020 Jun 1]. Available from: URL: https://www.vectornav.com/support/library/imu-and-ins.

37. SBG Systems. Ellipse 2 Series: MINIATURE HIGH PERFORMANCE Inertial Sensors; 2018 [accessed 2020 Apr 21]. Available from: URL: https://www.sbg-systems.com/wp-content/uploads/Ellipse_Series_Leaflet.pdf.

38. Inertial Labs. Precision Inertial Sensors and Systems: IMU, GPS-INS, AHRS, MRU [accessed 2020 Jun 1]. Available from: URL: https://www.unmannedsystemstechnology.com/company/inertial-labs/.

39. SBG Systems. Firmware Manual: Ellipse, Ekinox & Apogee High performance Inertial Sensors; 2019.

40. Lacey T. Chapter 11: Tutorial: The Kalman Filter: Massachusetts Institute of Technology.

41. Binns C. Aircraft systems: Instruments, communications, navigation, and control. First edition. Hoboken, NJ: John Wiley & Sons Inc; 2019.

42. Groves PD. Principles of GNSS, Inertial, and Multisensor Integrated Navigation Systems. Norwood, UNITED STATES: Artech House; 2013.

43. Xsens. Inertial Sensor Modules [accessed 2020 Jun 1]. Available from: URL: https://www.xsens.com/inertial-sensor-modules.

44. Xylem Inc. brand (Aanderaa). Motus Wave Sensor 5729: TD 316 OPERATING MANUAL; 2017 [accessed 2020 Jun 2]. Available from: URL: https://www.aanderaa.com/media/pdfs/td316-manual-motus-5729.pdf.

45. Xylem Inc. brand (Aanderaa). MOTUS Wave Sensor 5729; 2019 [accessed 2020 Jun 2]. Available from: URL: https://www.aanderaa.com/media/pdfs/d417_aanderaa_motus_wave_sensor_5729.pdf.

46. Leplomb H. SUCCESS STORY - Instrumented Buoys: Wave Buoys in the Arctic Sea Ice: SBG Systems; 2015.

47. Doble MJ, Bidlot J-R. Wave buoy measurements at the Antarctic sea ice edge compared with an enhanced ECMWF WAM: Progress towards global waves-in-ice modelling. Ocean Modelling 2013; 70:166–73.

48. Raghukumar K, Chang G, Spada F, Jones C, Janssen T, Gans A. Performance Characteristics of ‘‘Spotter,’’ a Newly Developed Real-TimeWave Measurement Buoy: Integral Consulting Inc.; Spoondrift Technologies Inc.; 2018.

49. Sofar Ocean. Spotter: Technical Specifications; 2019 [accessed 2020 Jun 2]. Available from: URL: https://content.sofarocean.com/hubfs/Spotter%20product%20documentation%20page/Sofar_Spotter_Specs_8_30_19.pdf?__hstc=17958374.8c952f59ebc2b51c152e9228a0f5bcc1.1581117931522.1581117931522.1581117931522.1&__hssc=17958374.3.1581117931522&__hsfp=2406343580.

50. Xsens. MTi 100-series: Overview [accessed 2020 Jun 2]. Available from: URL: https://www.xsens.com/products/mti-100-series.

51. Lars Thrane A/S. LT-500 AHRS: Product Sheet Rev. 1.03.

52. Zeng Z, Fa L. Accelerometer. In: Bobrowsky PT, editor. Encyclopedia of natural hazards: Includes case studies. Dordrecht: Springer Reference; 2013. p. 2 (Encyclopedia of Earth Sciences Series).

53. Bosch Mobility Solutions. Funktionsprinzip eines Beschleunigungssensors; 2018 [accessed 2020 Apr 1]. Available from: URL: https://www.youtube.com/watch?v=swCTbz5sIQM.

54. The Editors of Encyclopaedia Britannica. Accelerometer. In: Encyclopædia Britannica [accessed 2020 Apr 3]. Available from: URL: https://www.britannica.com/technology/accelerometer.

55. Bosch Mobility Solutions. Bosch MEMS-Sensoren: MEMS (mikro-elektro-mechanisches System) - Sensortechnologie im Chipformat [accessed 2020 Apr 1]. Available from: URL: https://www.bosch-mobility-solutions.com/de/produkte-und-services/industrie-und-bauelemente/mems-sensoren/.

56. OMEGA Engineering. Beschleuningungssensor: Einführung zum Thema Beschleunigungsmessung [accessed 2020 Apr 1]. Available from: URL: https://www.omega.de/prodinfo/beschleunigungsmesser-vibrationsaufnehmer.html.

57. OMEGA Engineering. Dehnungsmessstreifen DMS: Einführung zum Thema Dehnungsmessstreifen, DMS-Brücken [accessed 2020 Apr 3]. Available from: URL: https://www.omega.de/prodinfo/dehnungsmessstreifen-dms-bruecken.html.

58. Bernstein J. An Overview of MEMS Inertial Sensing Technology: Gyroscopes; 2003 [accessed 2020 Apr 6]. Available from: URL: https://www.fierceelectronics.com/components/overview-mems-inertial-sensing-technology.

59. Acar C, Shkel AM. MEMS Vibratory Gyroscopes: Structural Approaches to Improve Robustness. Berlin: Springer US; 2009. (MEMS Reference Shelf).

60. Silicon Sensing Systems Limited. MEMS Gyroscopes [accessed 2020 Apr 6]. Available from: URL: https://www.siliconsensing.com/technology/mems-gyroscopes.

61. Bosch Mobility Solutions. Bosch Funktionsprinzip eines Drehratensensors für ESP®; 2014 [accessed 2020 Apr 8]. Available from: URL: https://www.youtube.com/watch?v=6_yhOORMpc8.

62. The Editors of Encyclopaedia Britannica. Magnetometer. In: Encyclopædia Britannica [accessed 2020 Apr 9]. Available from: URL: https://www.britannica.com/technology/magnetometer.

63. Jayachandra Y. Smartphone frontiers: Technologies, applications and markets. New Delhi: Tata McGraw-Hill; 2014.

64. Azhagar Raj M, Janani P. Methods of Calculating B-Field at Hall Element in Open Loop Current Sensor: 2014 1st International Congress on Computer, Electronics, Electrical, and Communication Engineering (ICCEECE2014). In: IPCSIT vol. 59 (2014) © (2014) IACSIT Press, Singapore.

65. Nave R. Hall Effect: Georgia State University; 2018 [accessed 2020 May 20]. Available from: URL: http://hyperphysics.phy-astr.gsu.edu/hbase/magnetic/Hall.html.

66. Sharon Y, Khachatryan B, Cheskis D. Low current Hall Effect Sensor. Cornell University; 2018 Feb 8.

67. Joachim Herz Stiftung. HALL-Effekt: Grundwissen; 2020 [accessed 2020 May 20]. Available from: URL: https://www.leifiphysik.de/elektrizitaetslehre/bewegte-ladungen-feldern/grundwissen/hall-effekt.

68. Girgin A, Karalar TC. Output offset in silicon Hall effect based magnetic field sensors. Sensors and Actuators A: Physical 2019; 288:177–81.

69. Physics Department. Hall Effect: Boston University; 2019 [accessed 2020 May 20]. Available from: URL: http://physics.bu.edu/~duffy/semester2/d12_halleffect.html.

70. Hofmann-Wellenhof B, Lichtenegger H, Wasle E. GNSS - Global Navigation Satellite Systems: GPS, GLONASS, Galileo, and more. Vienna: Springer-Verlag Wien; 2008.

71. European GNSS Agency (GSA). What is GNSS?; 2017 [accessed 2020 May 5]. Available from: URL: https://www.gsa.europa.eu/european-gnss/what-gnss.

72. National Coordination Office for Space-Based Positioning, Navigation, and Timing. Other Global Navigation Satellite Systems (GNSS): NOAA; 2020 [accessed 2020 May 5]. Available from: URL: https://www.gps.gov/systems/gnss/.

73. Bundesamt für Kartographie und Geodäsie. Global Navigation Satellite Systems (GNSS); 2020 [accessed 2020 May 5]. Available from: URL: https://www.bkg.bund.de/DE/Observatorium-Wettzell/Messverfahren/Global-Navigation-System/global-navigation-system_cont.html.

74. National Coordination Office for Space-Based Positioning, Navigation, and Timing. How GPS works: NOAA [accessed 2020 May 5]. Available from: URL: https://www.gps.gov/multimedia/poster/poster-web.pdf.

75. Arnold T, Bertus MJ, Godbey J. A Simplified Approach to Understanding the Kalman Filter Technique. The Engineering Economist 2008; 53(2):140–55.

76. Meinhold RJ, Singpurwalla ND. Understanding the Kalman Filter. The American Statistician 1983; 37(2):123.

77. Faragher R. Understanding the Basis of the Kalman Filter Via a Simple and Intuitive Derivation [Lecture Notes]. IEEE Signal Process. Mag. 2012; 29(5):128–32.

78. Thrun S, Burgard W, Fox D. Probabilistic robotics. Cambridge, Massachusetts, London, England: MIT Press; 2006. (Intelligent robotics and autonomous agents series).

79. Ruhr-Universität Bochum. Das Kalman-Filter [Teaching Material]. Ruhr-Universität Bochum.

80. Applied Measurements. Load Cells | Force Sensors | Force Transducers | Load Measurement [accessed 2020 Apr 9]. Available from: URL: https://appmeas.co.uk/products/load-cells-force-sensors/.

81. Applied Measurements. Submersible Load Cell | IP68 | Underwater Force Sensor | DDEN: O-Ring Sealed, Fully Submersible, Accurate and Easily Adaptable [accessed 2020 Apr 9]. Available from: URL: https://appmeas.co.uk/products/load-cells-force-sensors/in-line-submersible-load-cell-dden/.

82. Svensson O, Leijon M. Peak Force Measurements on a Cylindrical Buoy With Limited Elastic Mooring. IEEE J. Oceanic Eng. 2014; 39(2):398–403.

83. Haddab Y, Chen Q, Lutz P. Improvement of strain gauges micro-forces measurement using Kalman optimal filtering. Mechatronics 2009; 19(4):457–62.

84. Cambridge University Press. Cambridge Advanced Learner's Dictionary & Thesaurus: Strain [accessed 2020 Apr 20]. Available from: URL: https://dictionary.cambridge.org/dictionary/english/strain.

85. National Instruments. Measuring Strain with Strain Gages; 2019 [accessed 2020 Apr 20]. Available from: URL: https://www.ni.com/sv-se/innovations/white-papers/07/measuring-strain-with-strain-gages.html.

86. National Instruments Corporation. Application Note 078: Strain Gauge Measurement – A Tutorial; 1998.

87. OMEGA Engineering. Strain Gauge: Introduction to Strain gauges [accessed 2020 Apr 9]. Available from: URL: https://www.omega.co.uk/prodinfo/StrainGauges.html.

88. Hottinger Baldwin Messtechnik GmbH. Wie funktioniert ein elektrischer Dehnungsmessstreifen?; 2018 [accessed 2020 Apr 20]. Available from: URL: https://www.hbm.com/de/7328/wie-funktioniert-ein-elektrischer-dehnungsmessstreifen/.

89. Arduino AG. Arduino Mega 2560 Rev3 [accessed 2020 May 31]. Available from: URL: https://store.arduino.cc/arduino-mega-2560-rev3.

90. Adeunis RF. ARF868 ULR & LR Radio modems [accessed 2020 May 31]. Available from: URL: https://www.texim-europe.com/getfile.ashx?id=102500.

91. Texas Instruments. MAX232xDual EIA-232Drivers/Receivers; 1989 [accessed 2020 May 7]. Available from: URL: http://www.ti.com/lit/ds/symlink/max232.pdf?ts=1588845859025.

92. lady ada. Micro SD Card Breakout Board Tutorial: Adafruit Industries, LLC; 2013 [accessed 2020 Jun 2]. Available from: URL: https://learn.adafruit.com/adafruit-micro-sd-breakout-board-card-tutorial/arduino-wiring.

93. Unger T, Blomqvist P. Teknisk-ekonomisk kostnadsbedömning av solceller i Sverige: Profu i Göteborg AB; 2018 [accessed 2020 Jun 7]. Available from: URL: http://www.energimyndigheten.se/globalassets/fornybart/solenergi/ovriga-rapporter/teknisk-ekonomisk-kostnadsbedomning-av-solceller-i-sverige.pdf.

94. Sveriges meteorologiska och hydrologiska institut (SMHI). Göteborg; 2014 [accessed 2020 Jun 8]. Available from: URL: https://www.smhi.se/polopoly_fs/1.90550!/Menu/general/extGroup/attachmentColHold/mainCol1/file/Daily_G%C3%B6teborg.png.

95. Alkhalidi AAT, Dulaimi NHA. Design of an Off-Grid Solar PV System for a Rural Shelter [Thesis]. Unpublished; 2018.

96. Chaar L. Solar Power Conversion. In: Rashid MH, editor. Power electronics handbook: Devices, circuits, and applications. 2nd ed. Amsterdam, Boston: Elsevier/AP; 2007. p. 661–72.

97. Qazi S. Portable Standalone PV Systems for Disaster Relief and Remote Areas. In: Qazi S, editor. Standalone photovoltaic (PV) systems for disaster relief and remote areas. Amsterdam, Netherlands: Elsevier; 2016. p. 113–38.

98. Ross JN, Kalogirou SA. System Electronics. In: Mcevoy's Handbook of Photovoltaics: Fundamentals and Applications. s.l.: Academic Pr; 2017. p. 765–88.

99. Victron Energy B.V. Welcher Solar-Lade-Regler: PWM oder MPPT?; 2014 [accessed 2020 May 29]. Available from: URL: https://prevent-germany.com/files/downloads/White-paper-Which-solar-charge-controller-PWM-or-MPPT-DE.pdf.

100. The Editors of Encyclopaedia Britannica. UHF. In: Encyclopædia Britannica [accessed 2020 May 20]. Available from: URL: https://www.britannica.com/technology/UHF.

101. Australian Radiation Protection and Nuclear Safety Agency. Radiofrequency radiation: Australian Government; 2014 [accessed 2020 May 20]. Available from: URL: https://www.arpansa.gov.au/understanding-radiation/what-is-radiation/non-ionising-radiation/radiofrequency-radiation.

102. Qualitative Reasoning Group. Communications System: Northwestern University [accessed 2020 May 20]. Available from: URL: http://www.qrg.northwestern.edu/projects/vss/docs/Communications/1-how-is-data-put-on-radio-waves.html.

103. Jones GA. National Association of Broadcasters Engineering Handbook, 10th Edition. [S.l.]: Focal Press; 2013.

104. The Editors of Encyclopaedia Britannica. Modulation. In: Encyclopædia Britannica [accessed 2020 May 20]. Available from: URL: https://www.britannica.com/technology/modulation-communications.

105. APPLIED MEASUREMENTS LTD. ICA Miniature Load Cell Amplifier; 2018 [accessed 2020 May 31]. Available from: URL: https://appmeas.co.uk/pdf/instrumentation/ICA.pdf.

106. Clas Ohlson. 12/24 V Solar Charge Controller: Model LS1024EU, Art. No. 36-6201; 2016 [accessed 2020 Jun 3]. Available from: URL: https://www.clasohlson.com/medias/sys_master/9542626934814.pdf.

107. SBG Systems. Quick Start Guide: Ellipse AHRS & INS [Miniature Inertial Systems]; 2018 2018 Apr 10.

108. National Marine Electronics Association. NMEA 0183 Interface Standard; 2018 [accessed 2020 May 30]. Available from: URL: https://www.nmea.org/content/STANDARDS/NMEA_0183_Standard.

109. SBG Systems. Hardware Manual: ELLIPSE 2 AHRS & INS High Performance, Miniature Inertial Sensors; 2018.

110. Arduino AG. Full pinout diagram Mega 2560 Rev 3; 2020 [accessed 2020 Jun 6]. Available from: URL: https://content.arduino.cc/assets/Pinout-Mega2560rev3_latest.pdf.

111. Dewey-Hagborg H. RS-232 [accessed 2020 Jun 6]. Available from: URL: https://www.arduino.cc/en/Tutorial/ArduinoSoftwareRS232.

112. Adeunis RF. User guide version 2.2.3, FRANCAIS, ENGLISH: ARF868 Radio Modems. Available from: URL: https://www.adeunis.com/wp-content/uploads/2019/09/ARF868_ARF794xx_RADIO_MODEMS_UG_V2.2.3_FR-GB.pdf.

8 Appendix

8.1 Lists of Components

8.1.1 List of Components – Recent State

As a result, from the system planning chapter it can be seen that following components are needed for the first build-up of the circuit (see Table 19):

Table 19: List of components.

Component	Name / further information	Company / further information
Inertial sensor unit	Ellipse2-D-G4A2-B1	SBG Systems
Cables Ellipse2-D	CA-ELI-RS232-CAN-3M	SBG Systems
Level converter	MAX232N	Texas Instruments
DIL 16 socket	For MAX232N	
1 µF capacitor	For MAX232N	
Arduino	Arduino Mega 2560	Arduino
Arduino USB cable	USB cable type A/B, standard USB 2.0 cable	Arduino
DC/DC converter	TEN 10-1212	TRACO Power
Micro SD-card	16 GB	
SD-card shield Arduino	Micro SD-card breakout board	Adafruit
Transmission system	RF ARF7940BA	Adeunis
IP67 Protection case	ACC1500AE	Adeunis
Power jack	ACC1500AA	Adeunis
Power supply	ACC1500AC	Adeunis
USB/RS232 bridge cable	ACC1500AB	Adeunis
D-sub cable	RND 765-00031	RND Connect
Wire / jumper cables / pin header / switches / amalgamating tape /silicone		
Solar panel for testing	SunWare 20163	SunWare
Charge controller	LS1024 EU	
Battery for testing	Varta 53030	Varta

8.1.2 List of Additional Components – Future Process

In Table 20 the components are listed that are already ordered or planned for the further process of the buoy:

Table 20: List of addition components for the later state of the project.

Component	Name / further information	Company / further information
Force transducer	DDENA2H-50kN-002-000	Applied Measurements
Antennas	PolaNt* MC	Septentrio Antennas, ordered with SBG Systems
Solar panel buoy	4x 15W PV panel	Open circuit voltage 20 V, Operational voltage: 18 V, Short circuit current: 21,8 A
Battery buoy	12 V, 60 Ah	Varta
Raspberry Pi	Raspberry Pi 3B+	Raspberry Pi
SD-card Raspberry Pi	With Raspberry Pi OS 2.1	Raspberry Pi
Power cable Raspberry Pi	5VDC, 2.5A, 13W	Raspberry Pi
Buoy	MB1200P, Monitoring buoy	Ningbo Botai Plastic Technology Co., LTD
Server	Unclear until this state of the project	Moxa Inc.

8.2 Programming

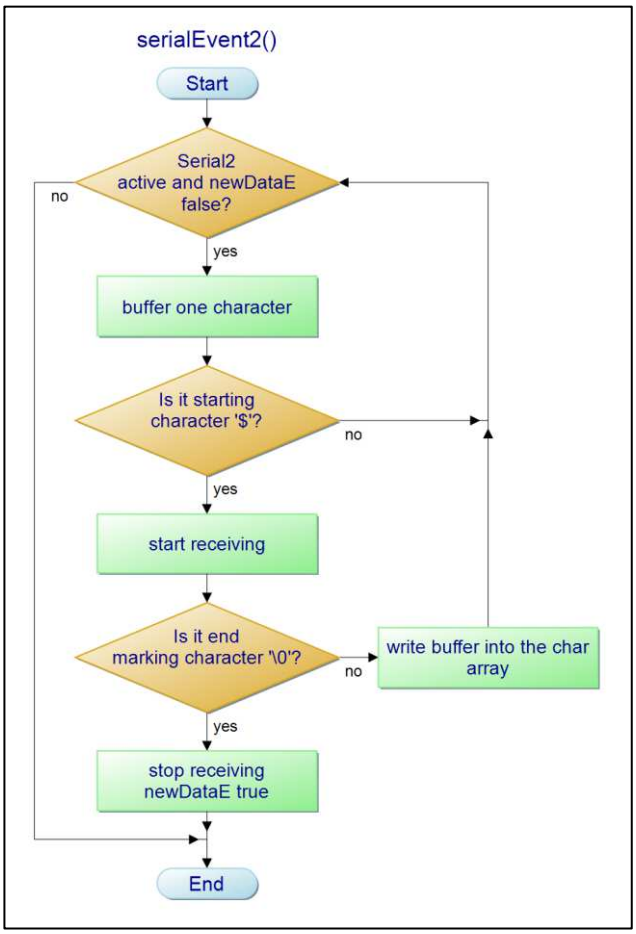

Figure 64: Flowchart of the serialEvent2() interrupt.

8.3 The Programming Code

```
/*
Juliana Lüer, 30.06.2020
*/

//SD-card
#include <SD.h>

//SD-card
File myFile;

//receiver arrays for the two sensor ports
const byte numChars = 200;
char RX_A[numChars];
char RX_E[numChars];

//indicator for new data
boolean newDataA = false;
boolean newDataE = false;

//_____________________________________________________________
//functions
void showA();
void showE();
void serialEvent1();
void serialEvent2();
void createnewfile();
void writeonSD();
void sendMessage();
//_____________________________________________________________

void setup()
{
  //fill receiving arrays with zeros
  memset(RX_A, '0', sizeof(RX_A));
  memset(RX_E, '0', sizeof(RX_E));

  // Open serial communications at 115200 baud
  Serial.begin(115200);
  Serial1.begin(115200);
  Serial2.begin(115200);
  Serial3.begin(115200);

  //enable Sensor communication
  // Check whether Serial1 is active
  if (Serial1.available())
     while (!Serial1)
     {
       ;
     }
  Serial.println("Serial 1 is active");

  // Check whether Serial2 is active
  if (Serial2.available())
     while (!Serial2)
     {
      ;
     }
  Serial.println("Serial 2 is active");

  // Check whether Serial3 is active
  if (Serial3.available())
     while (!Serial3)
     {
```

```
64        ;
65       }
66    Serial.println("Serial 3 is active");
67
68    //SD Card init
69    Serial.print("Initializing SD card...");
70    pinMode(53, OUTPUT); // CS is pin 53
71    if (!SD.begin(53))
72    {
73      Serial.println("initialization failed!");
74      return;
75    }
76    Serial.println("initialization done.");
77    myFile.close();
78  }
79
80  void loop()
81  {
82    //start routine if new Kalman model data (Port A) available
83    if (newDataA == true)
84    {
85       showA();                              //display on COM-port
86       sendMessage();                        //send via transmission system
87       newDataA = false;                     //indicator needs to be false again
88       memset(RX_A, '0', sizeof(RX_A));      //reset array to zero
89    }
90
91    //start routine if new raw data (Port E) available
92    if (newDataE == true)
93    {
94       showE();                              //display on COM-port
95       writeonSD();                          //store data on SD card
96       newDataE = false;                     //indicator needs to be false again
97       memset(RX_E, '0', sizeof(RX_E));      //reset array to zero
98    }
99  }
100
101
102 void showA()
103 {
104   //this function will print the output from Port A to the COM-port of the computer
105    Serial.print("A: ");
106    Serial.println(RX_A);
107 }
108
109
110 void showE()
111 {
112   //this function will print the output from Port E to the COM-port of the computer
113    Serial.print("E: ");
114    Serial.println(RX_E);
115 }
116
117 //receive on Port A via interrupt routine
118 void serialEvent1()
119 {
120     static boolean recvInProgressA = false;      //shows the state of the receiving
121 process
122     static byte ndxA = 0;                         //counts the index of the array
123     char startMarkerA = '$';                      //defines the start character of
124 the incoming NMEA command
125     char endMarkerA = '\n';                        //defines the end character of
126 the incoming NMEA command
127     char rc_A;                                    //read-out buffer
128
```

```
129     while (Serial1.available() && newDataA == false)
130      {
131          rc_A = Serial1.read();                     //read into buffer
132
133          if (recvInProgressA == true)               //request if receiving process
134  has started
135          {
136              if (rc_A != endMarkerA)                //enter if the command is still
137  going on
138              {
139                  RX_A[ndxA] = rc_A;                //go to the next array index and
140  write the character from the buffer in there
141                  ndxA++;                           //count for the next index +1
142              }
143              else                                    //enter if the command end is
144  reached
145              {
146                  RX_A[ndxA] = '\0';                //terminate the string
147                  recvInProgressA = false;          //end receiving process
148                  ndxA = 0;                          //reset the count for the array
149  index
150                  newDataA = true;                  //change the indicator
151              }
152          }
153          else if (rc_A == startMarkerA)           //enter if the starting character
154  in buffer
155          {
156              recvInProgressA = true;              //start receiving process
157          }
158      }
159  }
160
161  //receive on Port E
162  void serialEvent2()
163  {
164    static boolean recvInProgressE = false;       //shows the state of the receiving
165  process
166    static byte ndxE = 0;                          //counts the index of the array
167    char startMarkerE = '$';                        //defines the start character of
168  the incoming NMEA command
169    char endMarkerE = '\n';                       //defines the end character of the
170  incoming NMEA command
171    char rc_E;                                     //read-out buffer
172
173    while (Serial2.available() && newDataE == false)
174    {
175      rc_E = (char)Serial2.read();                 //read into buffer
176
177      if (recvInProgressE == true)                //request if receiving process has
178  started
179      {
180         if (rc_E != endMarkerE)                    //enter if the command is still
181  going on
182         {
183            RX_E[ndxE] = rc_E;                      //go to the next array index and
184  write the character from the buffer in there
185            ndxE++;                                //count for the next index +1
186          }
187          else                                   //enter if the command end is reached
188          {
189             RX_E[ndxE] = '\0';                  //terminate the string
190             recvInProgressE = false;            //end receiving process
191             ndxE = 0;                              //reset the count for the array
192  index
193             newDataE = true;                    //change the indicator
```

```
194         }
195      }
196       else if (rc_E == startMarkerE)             //enter if the starting character
197  in buffer
198       {
199          recvInProgressE = true;                //start receiving process
200       }
201    }
202  }
203
204  void sendMessage()
205  {
206    //this function will send a message via the transmitter
207    char msg[100];                              //data buffer
208    memset(msg, '0', sizeof(msg));              //reset data buffer (fill in zero)
209    sprintf(msg,"%s%c%c",RX_A,'\n','\0');    //sprint the receiving array into the
210  buffer and terminate the command with CR and LF
211    Serial3.print(msg);                         //send message to transmitter
212  }
213
214  void writeonSD()
215  {
216    //this function writes data on the SD-card
217    myFile = SD.open("test.txt", FILE_WRITE); //opens the file with the chosen name
218
219    if (myFile)                                 //writes in File, if it is opened
220    {
221      myFile.print(RX_E);                       //writing
222      myFile.close();                           //closes the file
223    }
224    else                                          //if the file didn't open, print an
225  error
226    {
227      Serial.println("error opening file");
228    }
229  }
```